JOURNAL OF PETROLOGY | VOLUME 51 | NUMBER 7 | PAGES 1477–1505 | 2010 | doi:10.1093/petrology/egq026

Field and Geochemical Constraints on Mafic–Felsic Interactions, and Processes in High-level Arc Magma Chambers: an Example from the Halfmoon Pluton, New Zealand

ROSE TURNBULL[1]*, STEVE WEAVER[1], ANDY TULLOCH[2], JIM COLE[1], MONICA HANDLER[3] AND TREVOR IRELAND[4]

[1]UNIVERSITY OF CANTERBURY, DEPRTMENT OF GEOLOGICAL SCIENCES, PRIVATE BAG 4800, CHRISTCHURCH 8140, NEW ZEALAND

[2]GNS SCIENCE, DUNEDIN RESEARCH CENTRE, PRIVATE BAG 1930, DUNEDIN, NEW ZEALAND

[3]VICTORIA UNIVERSITY OF WELLINGTON, SCHOOL OF GEOGRAPHY, ENVIRONMENT AND EARTH SCIENCES, WELLINGTON, NEW ZEALAND

[4]AUSTRALIAN NATIONAL UNIVERSITY, EARTH CHEMISTRY, CANBERRA ACT, 0200, AUSTRALIA

RECEIVED MARCH 31, 2009; ACCEPTED APRIL 29, 2010
ADVANCE ACCESS PUBLICATION JUNE 2, 2010

The ~140 Ma Halfmoon Pluton of Stewart Island, New Zealand, provides direct evidence for a number of physico-chemical processes that operate at depth within active arc settings. It is characterized by a sequence of mingled mafic sheets and enclaves that are preserved within intermediate–felsic host-rocks. Way-up structures and textures are consistent with a younging direction to the south, and allow a south-dipping magma chamber 'stratigraphy' to be constructed. The similarity in modal mineralogy, geochemistry, and isotopic signature between the various components, and their proximity in space and time, indicates that the system can be considered as a single composite pluton with discrete portions active at different times. Interpretation of mingling structures and textures in the field, combined with detailed geochemical and geochronological analyses, has allowed the identification of several physical and chemical processes operating within the chamber including: (1) multiple mafic magma pulses that were extensively mingled and sometimes physically mixed at the exposed level and at depth; (2) the development of mineral fabrics (e.g. aligned plagioclase and hornblende crystals) and alignment of mafic enclaves caused by processes of crystal accumulation, magmatic flow and compaction; (3) shortening of the chamber during crystallization as a result of magmatic loading; (4) fractional crystallization of the intermediate–felsic host magma that was interrupted periodically by mafic magma intrusion; (5) incremental assembly of the pluton from the base up; (6) limited chemical transfer between the mingled mafic sheets and enclaves and the surrounding intermediate–felsic host-rocks. Variations in morphology, chemistry and texture of the mingled mafic rocks relative to their position within the magmatic 'stratigraphy' indicate that processes operating within the chamber varied in both space and time. Mineral assemblages, chemical characteristics, primitive isotopic signatures and a lack of zircon inheritance indicate that the amphibole-rich, calc-alkaline Halfmoon Pluton was emplaced into a juvenile arc setting and experienced no contamination with ancient crustal materials. A model of pluton construction and evolution is presented that shows that the Halfmoon Pluton consisted of at least two adjacent magma pods that grew incrementally by episodic replenishments of mafic magma into a magma chamber of evolving intermediate–felsic composition. Data are consistent with a model whereby hydrous amphibole-rich basaltic magmas ponded at the crust–mantle interface and episodically rose, injected and mingled

*Corresponding author. E-mail: rose.turnbull@canterbury.ac.nz

with an overlying intermediate–felsic magma chamber that itself represented the fractionated product of the same basaltic mantle melts.

KEY WORDS: *crystal accumulation; granite; mafic replenishment; magma chamber; magma mingling*

INTRODUCTION

Understanding the processes that operate within 'magma chambers' is crucial towards answering fundamental questions about how the crust is formed and evolves over time. The origin and evolution of silicic magmas in arc settings is a continuing topic of debate (Arculus, 1994; Tamura & Tatsumi, 2002; Smith *et al.*, 2003, 2006; Shukuno *et al.*, 2006; Wright *et al.*, 2006; Tamura *et al.*, 2009). Magmas produced in arc settings rarely represent primary mantle-derived melts, more typically displaying differentiated compositions reflecting such processes as magma mixing, fractional crystallization and crustal assimilation. Clues to the processes that operate within arc settings can be found in exposed sections of arc crust, which provide direct field evidence for the physico-chemical processes that operate within magma chambers and lead to the bulk structure and composition of arc crust.

Plutonic rocks have long been overlooked in favour of studying volcanic deposits because of a long-held view that plutonic bodies are monotonously homogeneous, and that the magmatic processes that operated within them are no longer preserved, having been eliminated by near-solidus processes. Work by several researchers (Frost & Mahood, 1987; Blundy & Sparks, 1992; Wiebe, 1993*a*, 1993*b*, 1994; Coleman *et al.* 1995; Wiebe & Collins, 1998; Bachl *et al.*, 2001; Miller & Miller, 2002; Harper *et al.*, 2004; Perugini *et al.*, 2005; Collins *et al.*, 2006; Kamiyama *et al.*, 2007; Walker *et al.*, 2007) over the last two decades has shown, however, that plutonic bodies are often internally highly variable and contain structures and textures that formed through the complex interplay between several petrogenetic processes. This is no more evident than in composite mafic–silicic layered intrusions that contain evidence for the coeval interaction between two or more magmas of contrasting composition and physical properties, which typically preserve an integrated record of prolonged magmatic evolution, including pluton accumulation, crystallization and emplacement within the crust. By studying the magmatic history of composite plutons, insights can be gained into the physical, chemical and thermal processes responsible for the formation of plutons in a variety of tectonic settings, and conclusions drawn on the size and longevity of magmatic systems, rates of pluton construction, and the origin of magma source regions.

Work by several researchers has indicated that plutons may form incrementally as a result of multiple intrusions of magma of both similar and contrasting composition, with different portions of the chamber active at different times (Coleman *et al.*, 1995; Wiebe, 1996; Wiebe & Collins, 1998; Glazner *et al.*, 2004; Lipman, 2007). These plutonic bodies may also be long-lived, of the order of millions of years, remaining active through the episodic replenishment of both mafic and felsic magmas (Davies *et al.*, 1994; Bachl *et al.*, 2001; Jellinek & DePaolo, 2003; Coleman *et al.*, 2004; Glazner *et al.*, 2004; Harper *et al.*, 2004; Hawkins & Wiebe, 2004; Walker *et al.*, 2007). Incrementally constructed plutons occur in a variety of tectonic settings, and they are characterized by evidence of basaltic magma injecting and mingling with felsic magma. Examples include plutons from the Coastal Maine Magmatic Province (Wiebe, 1993*a*, 1994; Wiebe *et al.*, 2001), Aztec Wash Pluton (Harper *et al.*, 2004), Spirit Mountain Batholith (Walker *et al.*, 2007), and the Tottabetsu Plutonic Complex (Kamiyama *et al.*, 2007). The Halfmoon Pluton of Stewart Island, New Zealand has been recognized as part of an island arc (Muir *et al.*, 1998) and offers a rare opportunity to examine a composite pluton that was generated within an arc setting. Physical and chemical processes identified within the exhumed Halfmoon Pluton hold important clues to the petrogenetic processes that operate within active arc settings, and further our understanding of the genesis and evolution of arc-related plutonic and volcanic rocks.

GEOLOGY OF THE HALFMOON PLUTON

The Halfmoon Pluton occurs within the composite Bungaree Intrusives (Allibone & Tulloch, 2004), which crop out in an ~2–8 km wide strip exposed along the northern coast of Stewart Island (Fig. 1). The magmas represented by these intrusions were emplaced ~175–140 Myr ago along the convergent New Zealand margin of Gondwana, and they dominate the outboard part of the Median Batholith (Kimbrough *et al.*, 1994; Mortimer *et al.*, 1999; Tulloch & Kimbrough, 2003). The Median Batholith represents a belt of mainly subduction-related I-type plutonic rocks of Carboniferous to Early Cretaceous age that separates the Eastern and Western Provinces of New Zealand (Tulloch & Kimbrough, 2003). The outboard margin of the Median Batholith is dominated by plutonic rocks of the Darran Suite, which encompasses all mafic and felsic plutonic rocks in eastern Fiordland with ages between 168 and 137 Ma (Muir *et al.*, 1998). The I-type Darran Suite has calc-alkaline chemistry, zircon populations and an isotopic character that suggests little involvement with pre-Carboniferous continental rocks (Allibone *et al.*, 2009). It is interpreted to have been

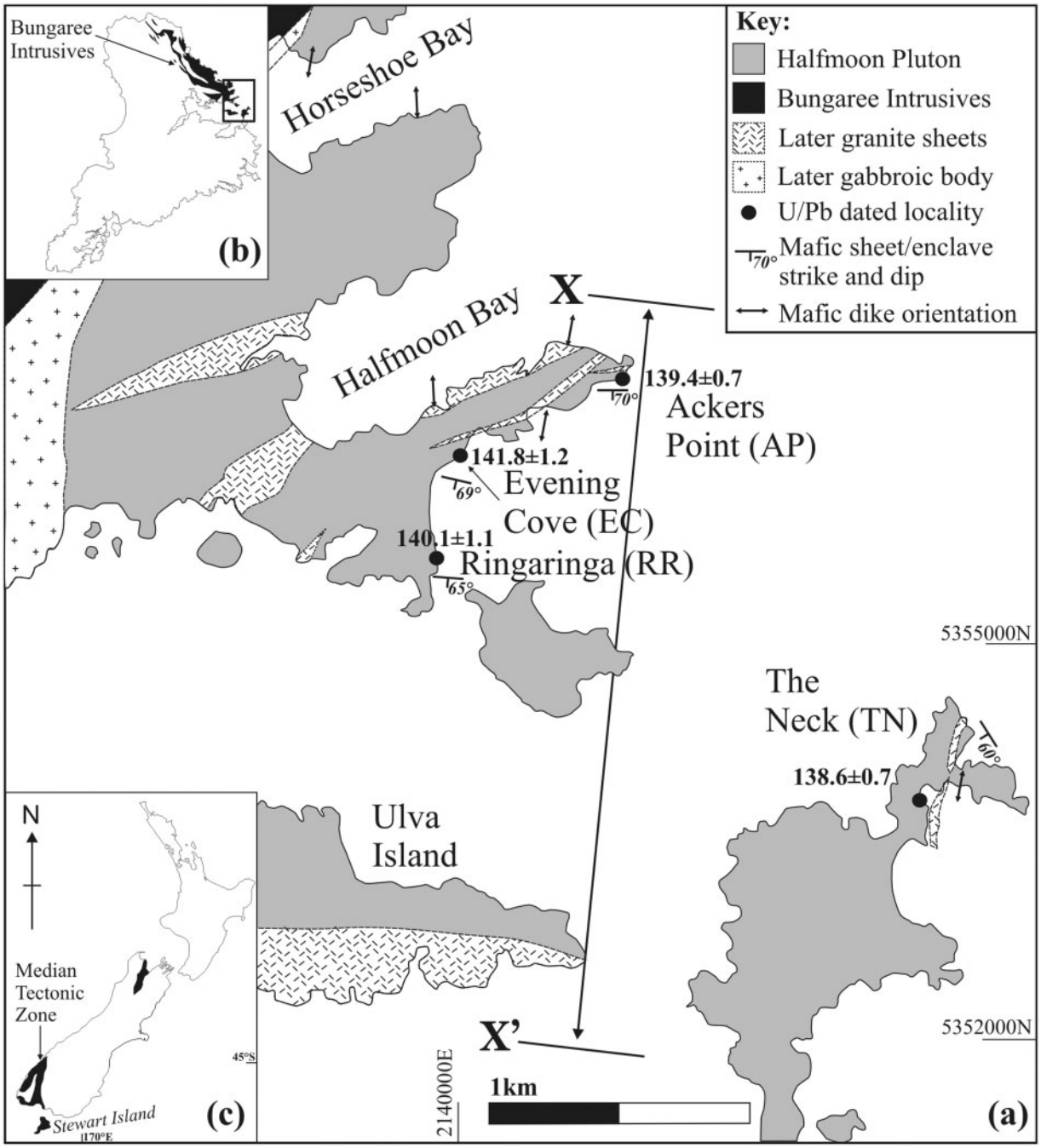

Fig. 1. (a) Simplified geological map of the Halfmoon Pluton and relationship with other plutonic bodies within the Bungaree Intrusives. Cross-cutting mafic dikes all intrude perpendicular to the strike and dip of mafic sheets and enclaves. X represents the inferred base of the chamber, and X' the inferred top of the chamber. (b) Map of Stewart Island indicating the full extent of the Bungaree Intrusives as mapped by Allibone & Tulloch (2004). (c) Map of New Zealand showing the extent of the Median Batholith (modified from Mortimer *et al.*, 1999).

derived from melting in the mantle wedge above a subducting slab of oceanic lithosphere (Muir *et al.*, 1998). The Darran Suite contains field evidence for mafic–felsic interaction, and has similar rock types, geochemistry, age and isotopic signatures to the Bungaree Intrusives; these have been interpreted by several workers to be correlatives (Allibone & Tulloch, 2004; Allibone *et al.*, 2009).

Previous work (Watters, 1978; Cook, 1988; Wiebe & Collins, 1998; Smith, 2000; Allibone & Tulloch, 2004) has illustrated the heterogeneous nature of the Bungaree

Intrusives, and highlighted the potential for further study of the magma mixing and mingling structures that occur. The Bungaree Intrusives exposures west of Halfmoon Bay are small and discontinuous, and represent an older suite of plutonic rocks, whereas exposures east of Halfmoon Bay are larger and more continuous, and represent a single pluton within the larger composite Bungaree Intrusives. This pluton, as outlined in Fig. 1 is referred to below as the Halfmoon Pluton (new name). Areas chosen for detailed structural, textural, geochemical and geochronological study within the pluton were based on accessibility and the nature of coastal exposures. This pluton was chosen for detailed study because it crops out extensively enough to ensure that detailed structural and textural interpretations of the mingled rocks can be made across distances of between ~5 and 50 m. No pluton margins are exposed; however, the inferred base of the pluton lies close to the north side of Horseshoe Bay (Fig. 1). The sections chosen for detailed study from Ackers Point to The Neck occur at right angles to the strike of the magmatic layering, thus offering cross-sections through the pluton. Outcrops are generally limited in lateral extent, with outcrop widths typically between 4 and 20 m.

FIELD RELATIONSHIPS AND PETROGRAPHIC CHARACTERISTICS

The Halfmoon Pluton is characterized by a sequence of mafic sheets and enclaves of basaltic composition which occur as layers within a more intermediate–felsic host (leucodiorite–granodiorite–tonalite). Mafic rocks have textures similar to pillow basalts, with fine-grained 'quenched' margins and coarser-grained centres, indicating that they chilled rapidly against the cooler, more felsic, host-rocks. Consistent dip directions of sheets and enclaves reveal that the magma chamber as a whole has been tilted ~70° from the horizontal towards the south, exposing a cross-section through the pluton and allowing for interpretations to be made with respect to height or depth within the chamber. Four key sections were chosen for detailed structural and textural analysis based on field exposures and position within the stratigraphic sequence: Ackers Point (AP), Evening Cove (EC), Ringaringa (RR) and The Neck (TN) (see Fig. 1 for locations). Each of these areas exhibits varied mingling styles, textures and compositions, as shown in Figs 2 and 3.

Magma chamber 'stratigraphy' and way-up indicators

A magmatic 'stratigraphy' was constructed through recognition of way-up indicators and depositional structures within the mingled rocks. The most abundant and reliable way-up structures identified within the Halfmoon Pluton are fine-grained quenched basal contacts of mafic sheets that exhibit numerous flame structures and load casts (Fig. 2d)—structures analogous to younging indicators in sedimentary rocks. Flame structures were interpreted by Wiebe & Collins (1998) to form as a result of dense mafic sheets sinking into more buoyant felsic magma, which rises and injects into the base of the mafic sheet. Mafic sheets and enclaves all preserve a pervasive preferred orientation striking between 085° and 110°, indicating that the vertical extent of the magma chamber is in a north–south direction. Other distinctive field relationships that can be used to infer way-up include cross-cutting relationships; sinking of denser mafic sheets and enclaves towards the base (Fig. 2e); mafic feeder dikes that cross-cut earlier-formed mafic enclaves and then spread laterally and mingle with the felsic host (Fig. 2a); concentrations of amphibole beneath chilled mafic sheets, and vugs containing coarse-grained amphibole and plagioclase within flame structures as a result of the vertical escape of volatiles (Fig. 2c); felsic layers with laminated feldspars and faint modal layering indicative of cumulates. Many of these mingling structures and textures have been identified in several well-studied composite plutons worldwide (Wiebe & Collins, 1998; Bachl *et al.*, 2001; Harper *et al.*, 2004; Collins *et al.*, 2006; Kamiyama *et al.*, 2007) and have been used as evidence to suggest that plutons are constructed incrementally from the base up. Way-up structures in mafic sheets and enclave swarms within the Halfmoon Pluton are consistent throughout the sequence and all point towards the south (Fig. 2). The inferred base of the plutonic body was therefore identified at Ackers Point, and the inferred top at The Neck (Fig. 1), providing a minimum pluton thickness of at least 4·8 km. The width of the complex is difficult to determine because it extends beneath the sea; however, a minimum width of ~6·5 km has been measured.

Mingling structures and characteristics

The style of magma mingling varies considerably within the Halfmoon Pluton. Ackers Point represents the lowermost exposed section of the pluton, and is inferred to represent the base. This section consists of thick (8–15 m) mafic sheets separated by thin (<1 m) portions of intermediate (leucodiorite) host-rock. The mafic sheets have an average preferred orientation and dip of 089/70° and display fine-grained chilled margins and coarser-grained centres. Evening Cove sits stratigraphically above Ackers Point, and is characterized by a sequence of at least six thick (1–10 m) mafic sheets and enclave swarms that are separated by ~1–3 m sections of intermediate (leucodiorite) host-rock (Fig. 4). Mafic sheets and enclaves have an average orientation and dip of 107/70°. Mafic sheets within this section display the characteristic morphology as outlined by Wiebe & Collins (1998), with a fine-grained quenched basal contact, coarser-grained centres, and

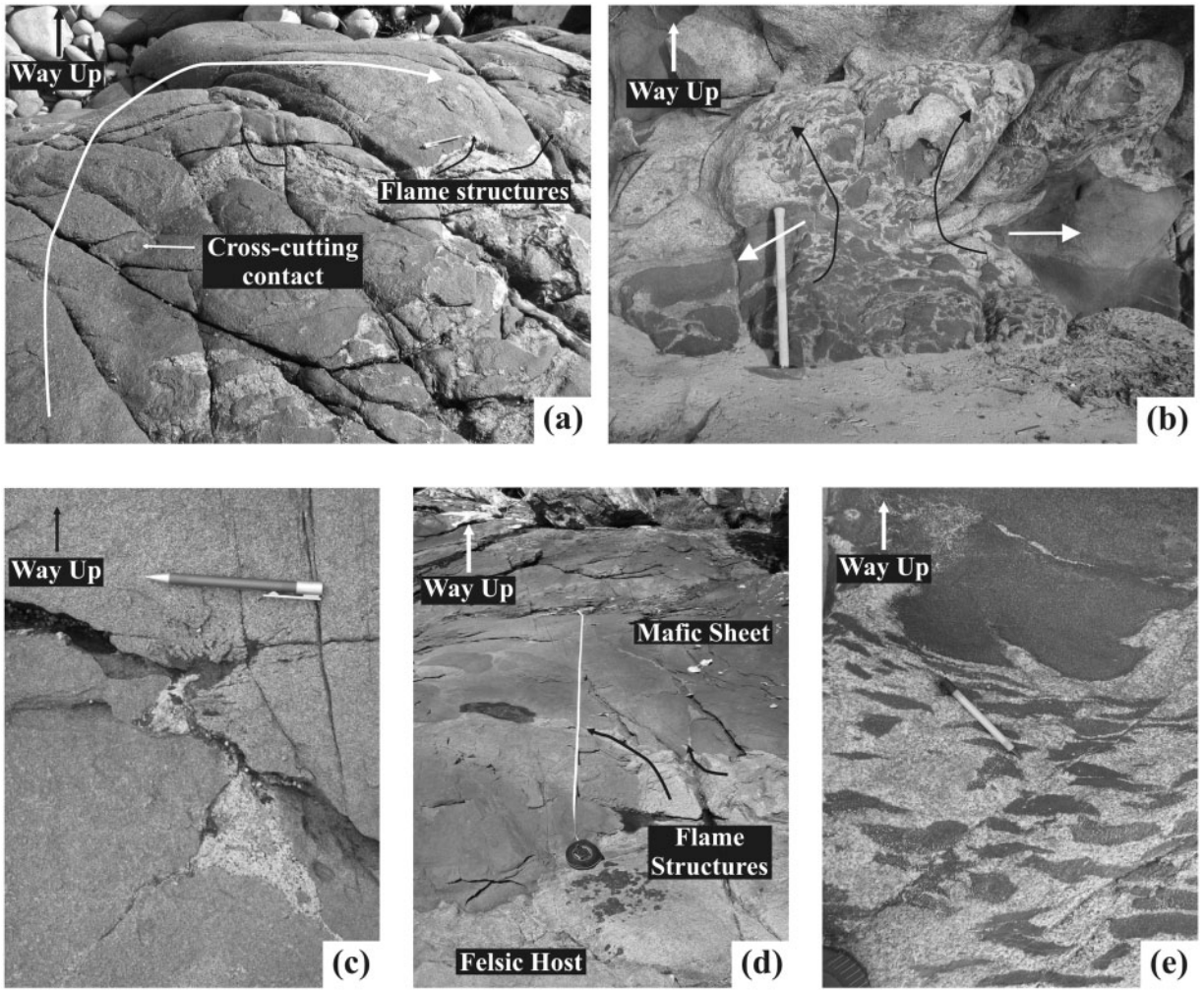

Fig. 2. Way-up structures identified within the Halfmoon Pluton. (a) Mafic feeder-dike cross-cutting mafic enclaves to the left of the photograph, spreading laterally at the top of photograph where it mingles with the surrounding host. (b) Vertical flow of mafic enclaves breaking apart a mafic sheet. (c) Concentration of amphibole at the top of a flame structure formed as a result of the vertical escape of volatiles. (d) Fine-grained chilled base of a mafic sheet with several flame structures that have risen vertically into the base of the sheet. (e) Flow-aligned mafic enclaves being compressed beneath a sinking mafic sheet (at the top of the photograph).

gradational, enclave-rich rubbly tops (Fig. 3a). Several mafic enclaves have gradational contacts and evidence for the mechanical exchange of crystals from the host into the mafic rock, indicating that a degree of mixing occurred between the mafic and felsic magmas. Mafic enclaves that are much lighter in appearance and have diffuse margins are evidence for more thorough mixing between the mafic and felsic materials (Fig. 3e). A detailed sketch of the section exposed at Evening Cove is shown in Fig. 4.

Mingling structures at Ringaringa beach (Fig. 1) consist of thin (0·5–2 m) laterally discontinuous mafic sheets alternating with concentrated enclave swarms that are separated by a felsic (granite–granodiorite) host (Fig. 3c). Enclave size and shape remain relatively consistent throughout the section, and occur in swarms, which probably reflects their original emplacement as mafic sheets. Orientations within the mafic enclaves and sheets are very consistent within this section, with an average orientation and dip of 097/65°. Mechanical mixing on a local scale is evident, with several small (5 cm × 10 cm) mafic enclaves containing xenocrysts of plagioclase and quartz that are probably derived from the felsic host.

The Neck is a low-lying peninsula that represents a large, almost continuously exposed section of ~1 km. The coeval interaction of mafic and felsic magmas at The Neck has resulted in the formation of a thick, uninterrupted succession of aligned mafic enclaves (Fig. 3d) within an intermediate–felsic (tonalite) host-rock. The size, shape and degree of concentration of the mafic enclaves varies

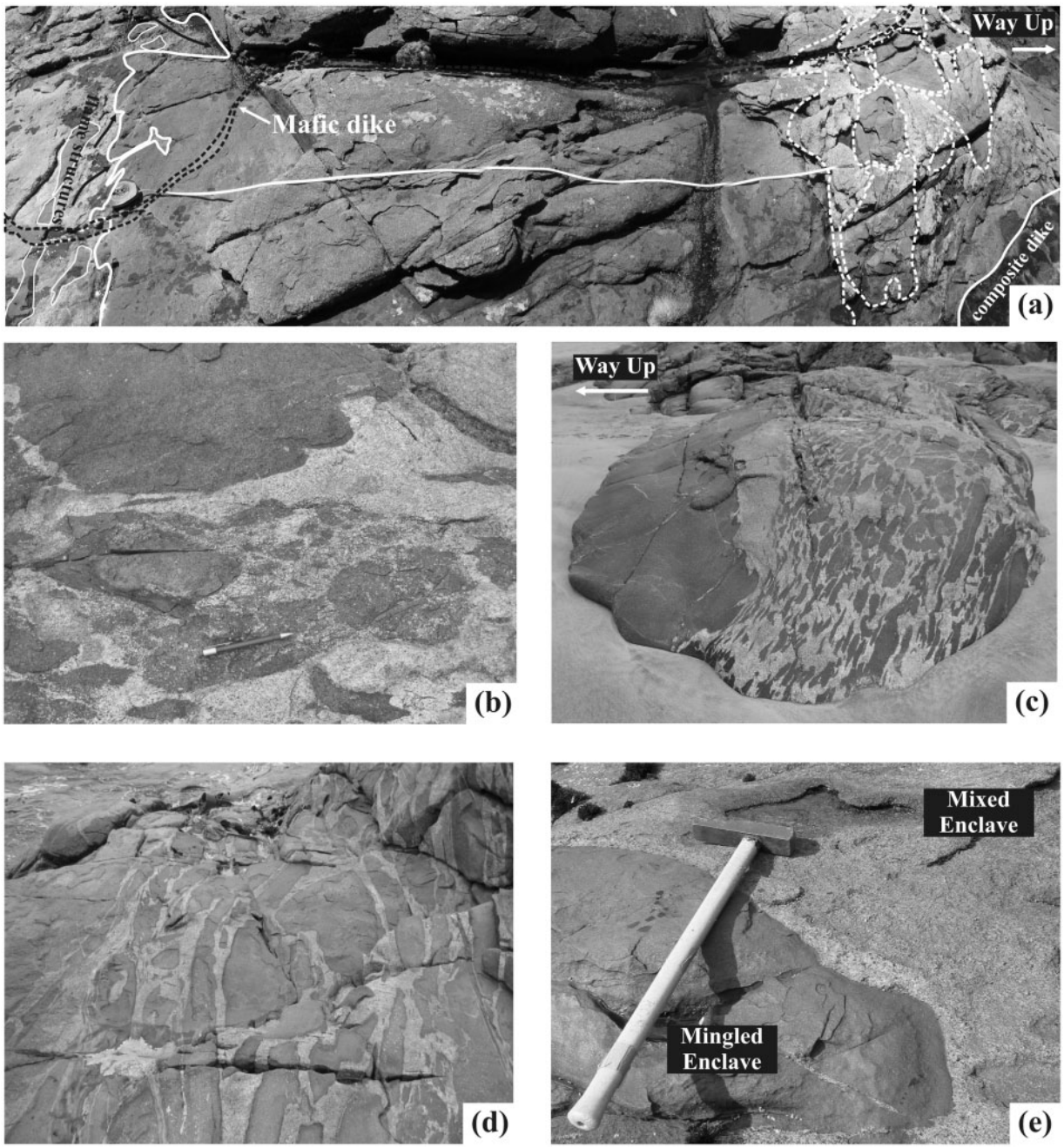

Fig. 3. Photographs illustrating the different styles of mafic–felsic interaction within the Halfmoon Pluton, and where recognized, way-up. (a) Mafic sheet ~3·6 m in width and at least 9 m in length. The photograph displays the typical morphology of a mafic sheet with a chilled base (at left) punctuated by flame structures, and a gradational, rubbly top with numerous enclaves (at right). (b) 'Composite' enclave that mingled elsewhere prior to emplacement at its current site. (c) Mafic enclave swarm and overlying mafic sheet at Ringaringa. Numerous flame structures at the base of the sheet should be noted. (d) Typical mafic enclave swarm at The Neck. (e) Mixing on a local scale. Mingled mafic enclave on the left, with a highly mixed mafic enclave on the right displaying a gradational boundary with the felsic host-rock.

considerably. Mafic enclave orientations within this section are at an angle to the other three sections, with average orientations and dips of 147°/60°. Towards the south (inferred top of the chamber), these orientations become more concordant with those at the other locations, with average orientations and dips of 110°/60°. Composite enclaves are present at several locations (Fig. 3b), and consist of mixed mafic and felsic material that has mingled with

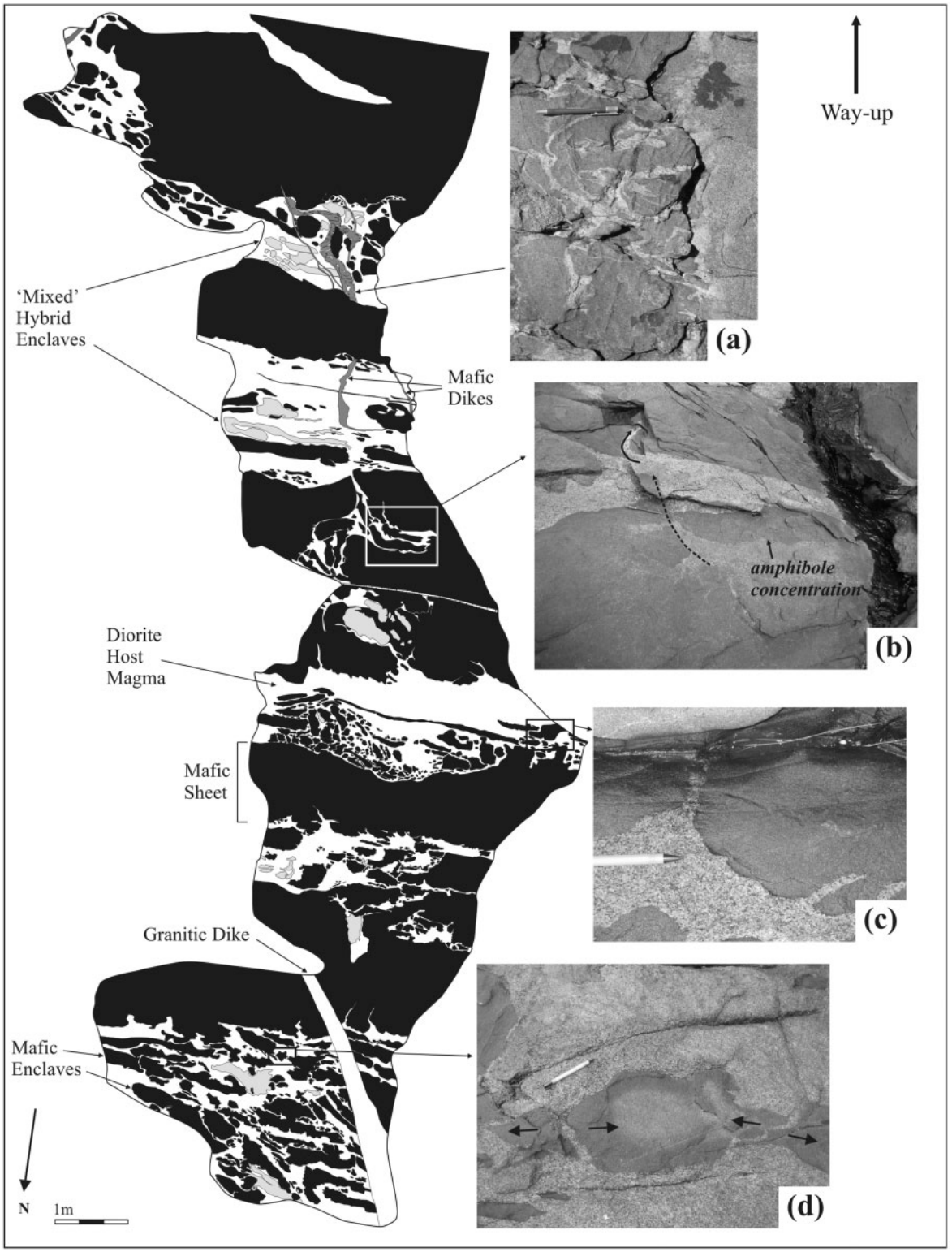

Fig. 4. Section exposed at Evening Cove. The section is oriented with top to the south to highlight way-up within the magmatic 'stratigraphy' The pervasive east–west strike of the sheets and enclaves throughout the entire section should be noted. (a) Composite dike. (b) Top of mafic sheet showing an amphibole concentration as a result of the escape of volatiles. Volatiles have pushed through the top of the sheet and into the base of the sheet above. (c) Crenulate margin of a mafic enclave as a result of shortening within the chamber in the north–south direction. (d) Thin mafic sheet that has been pulled apart to form mafic enclaves.

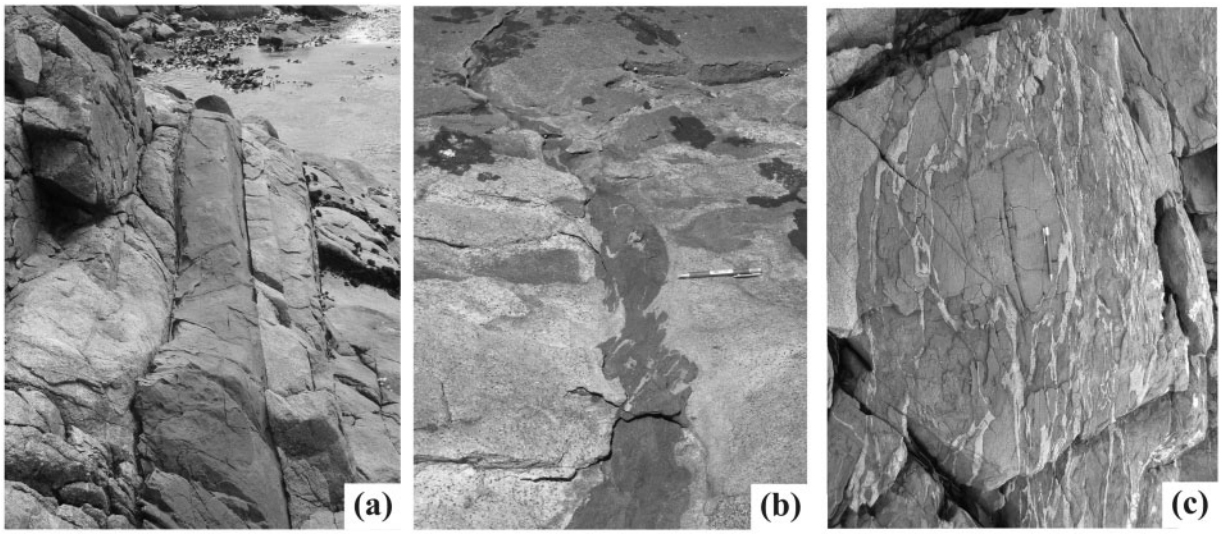

Fig. 5. Styles of mafic dike emplacement. (a) Mafic magma injected when the host was completely solidified. No physical or chemical interaction occurs between the two rocks. (b) Mafic dike injected when the felsic host still contained some heat or melt, allowing for limited physical and chemical exchange. (c) Composite dike formed by the remobilization and incorporation of residual felsic magma into the intruding mafic dike.

the surrounding host, indicating that they were still mushy when emplaced.

Several mafic dikes cross-cut the Halfmoon Pluton, and differences in the form of these dikes indicate variable extents of crystallization of the host magma when the dikes were intruded. Mafic dikes with sharp, well-defined edges that cross-cut all foliations and crystals within the host-rocks appear to have intruded when the pluton was completely solidified (Fig. 5a). Mafic dikes with diffuse, gradational edges, which commonly meander through the host-rock and bend around relatively rigid objects such as mafic sheets and enclaves, or have pulled apart upon entry (Fig. 5b), were likely to have been intruded when the host magma retained enough interstitial melt to allow plastic deformation of these dikes (Wiebe, 1993*a*). Composite dikes (Fig. 5c), where mafic enclaves are enclosed within a felsic matrix, also occur within the pluton, although these are concentrated in swarms towards the top of the chamber. Composite dikes have been interpreted by several researchers to inject contemporaneously with pluton crystallization, with residual or interstial felsic melt incorporated into the composite dike by the intruding mafic magma (Wiebe, 1973; Snyder *et al.*, 1996; Wiebe & Ulrich, 1997). The presence of mafic dikes with varying forms and compositions, injected during different stages of pluton crystallization, is evidence for the continuous input of mafic magma into the magma chamber throughout its crystallization history.

Petrography of Halfmoon Pluton

The intermediate–felsic host-rocks are medium-grained (1–5 mm), with compositions ranging from a hornblende leucodiorite at the inferred base of the chamber (AP and EC), to a biotite granite (RR), and finally a biotite tonalite towards the inferred top of the chamber (TN). Modal analyses were determined by counting 500 points on thin sections. Plagioclase, hornblende and biotite crystals were analyzed by electron microprobe to determine their composition. Representative compositions of these minerals are given in Table 1.

Host-rocks towards the inferred base of the chamber (AP and EC) are dominated by high modal proportions of plagioclase (68–90%), which occur as aligned, tabular crystals that define a cumulate texture. Plagioclase has a composition between An_{30} and An_{42}. Hornblende (5–12%) is almost always euhedral, olive–green pleochroic, is commonly twinned and is aligned parallel to the plagioclase crystal alignment. Hornblendes are classified as magnesio-hornblendes (Leake *et al.*, 1997), with MgO contents of 12–14 wt %. Biotite (<1–6%) is euhedral to subhedral, straw–brown pleochroic and appears to be a late crystallizing phase. Biotites have FeO contents of ~19 wt % and MgO contents of ~12 wt %. Quartz (0–5%) is anhedral and interstitial. Zircon crystals are relatively abundant, euhedral and typically occur in the interstices between plagioclase and hornblende. Fe–Ti oxides (<1–3%) typically occur as euhedral cubic-shaped crystals, indicating that they are probably magnetite. Titanite (trace) occurs either interstitially or as anhedral rims around Fe–Ti oxides, indicating that it is a late crystallizing phase. Apatite is euhedral and occurs either as inclusions within plagioclase as stubby prisms or as acicular crystals. Host-rocks towards the inferred top

Table 1: Representative major element analyses of hornblende, plagioclase and biotite from the Bungaree Intrusives

Type:	Plagioclase				Biotite				Hornblende		
Sample:	AP#G	EC 1/6	TN#17	Sample:	AP#G	EC 1/6	TN#17	Sample:	AP#G	EC 1/6	TN#17
SiO_2	57·36	58·81	58·79	SiO_2	36·94	36·58	37·06	SiO_2	46·8	47·09	47·87
Al_2O_3	26·92	26·57	26·23	Al_2O_3	15·88	15·75	15·42	TiO_2	1·01	1·02	0·82
FeO	0·10	0·25	0·19	FeO	18·68	20·02	18·31	Al_2O_3	7·85	7·67	6·92
CaO	8·66	7·74	7·71	MnO	—	0·36	0·26	FeO	14·93	15·33	14·3
Na_2O	6·53	7·08	7·07	MgO	11·58	11·19	12·09	MgO	12·95	12·52	13·57
K_2O	0·07	0·15	0·16	Na_2O	0·21	—	—	MnO	0·51	0·52	0·42
Total	99·64	100·60	100·15	K_2O	8·83	8·85	8·88	CaO	11·62	11·7	12·19
%An	42·12	37·34	37·26	TiO_2	3·64	2·73	3·85	Na_2O	1·08	0·97	0·87
%Ab	57·47	61·81	61·81	Cl	0·08	—	0·09	K_2O	0·41	0·54	0·35
%Or	0·41	0·41	0·92	Total	95·84	95·48	96·10	Total	97·16	97·36	97·31

Samples AP#G and EC1/6 represent felsic host; sample TN#17 represents the mafic component of a composite dike.

of the chamber (RR and TN) contain smaller proportions of randomly oriented sub- to euhedral plagioclase feldspar (14–87%) and higher proportions of quartz (6–47%), which becomes more subhedral as it increases in abundance towards the inferred top of the chamber. Plagioclase has a composition between An_{26} and An_{35}. Alkali feldspar (<1–37%) is subhedral, and occurs in almost all host-rocks from Ringaringa but only one host-rock from The Neck. The dominant mafic phase changes within the host-rocks at Ringaringa and The Neck from hornblende to biotite. Where hornblende is present (2–11%) it occurs as subhedral grains; it is classified as magnesio-hornblende. Biotite (1–12%) is brown pleochroic and sub- to euhedral; where it occurs in the same rock with hornblende it is typically intergrown, forming in clots. Biotite crystals have FeO contents of ~21 wt % and MgO contents of ~10 wt %. Accessory apatite, titanite and Fe–Ti oxides occur in abundances <1–2%. Zircon crystals are euhedral and are most commonly found as inclusions within biotite, displaying pleochroic haloes. Scarce secondary phases of chlorite, sericite and myrmekite are present in abundances of 0–1% in all host-rocks in the Halfmoon Pluton.

All of the mafic rocks (sheets, enclaves, dikes) are classified petrographically as hornblende mesodiorites (Streckeisen, 1973). The quenched margins of mafic sheets and mafic enclaves are fine-grained (~0·5 mm), becoming coarser-grained towards their centres; the mafic sheets are typically <1·5 m thick with crystal sizes ranging from 1 mm to 2 mm. Mafic sheets and enclaves are characterized by ~60% mafic minerals (hornblende and/or biotite), ~35% plagioclase, and <5% Fe–Ti oxides and titanite. Mafic enclaves often contain between 0·5 and 1% modal apatite, which is often acicular. Subhedral xenocrystic quartz and plagioclase crystals are sometimes included within the mafic rocks. As in the intermediate–felsic host-rocks, the dominant mafic phase changes from hornblende to biotite towards the inferred top of the chamber. Hornblende-bearing mafic rocks are enclosed within hornblende-bearing host-rocks, whereas biotite-bearing mafic rocks are enclosed within biotite-bearing host-rocks. Hornblende, where present, is green pleochroic, euhedral, and typically occurs in clots. Biotite crystals are brown pleochroic, euhedral, and often occur as blades. Plagioclase crystals are typically euhedral, and often define a weak preferred orientation parallel to that of the sheet and enclave orientation. Plagioclase compositions range from An_{43} at the inferred base of the chamber (AP) to An_{39} towards the inferred top (TN). The An composition of plagioclase within the mafic sheets and enclaves is very similar to that in the surrounding host, usually only greater by 1–2%.

Mixed 'hybrid' rocks were identified as such based on their appearance in the field, and their petrography and geochemistry (see geochemistry section). In the field, rocks that are interpreted to have undergone mechanical mixing with the surrounding host display colours intermediate to the light intermediate–felsic host-rocks and the dark mafic sheets and enclaves (Fig. 3e). They also typically display diffuse contacts with evidence of exchange of crystals with the surrounding host-rock. Petrographically they contain a mixture of fine- and coarser-grained crystals derived from both the mafic and felsic rocks, and have the same modal mineralogy as the unmixed rocks that enclose them.

Mafic dikes are typically characterized by the same modal mineralogy as the mafic sheets and enclaves, although they are usually more hornblende and Fe–Ti oxide-rich, and are much finer-grained (0·1–0·2 mm). Plagioclase crystals are typically lath-like, are coarser grained than the mafic minerals, and are strongly foliated parallel to the margins of the dikes. Several mafic dikes are characterized by clots of magnesio-hornblende that form in subhedral shapes that are aligned parallel to the margins of the dike. Composite dikes are characterized by fine-grained (0·1–0·2 mm) mafic enclaves within a fine-grained felsic host (0·2–0·4 mm) (Fig. 5c). Biotite crystals within the mafic component of the composite dikes have the least evolved compositions within the Halfmoon Pluton rocks, with FeO contents of ~18 wt % and MgO of ~13 wt % (sample TN#17, Table 1). The felsic host is typically coarser-grained that the mafic enclaves it encloses. The contact between the mafic and felsic rocks is typically very sharp and planar, although felsic material often penetrates into the mafic enclaves and seems to mix slightly with the mafic material (Fig. 3d), indicating that both the mafic and felsic components of these dikes were liquid at the same time.

ANALYTICAL METHODS

Seventy-four samples were selected for whole-rock major and trace element analysis. From these, eight samples were selected for analysis by electron microprobe, 14 samples were chosen for Sr–Nd isotopic analysis, and five samples were chosen for U/Pb sensitive high-resolution ion microprobe (SHRIMP) dating.

Fresh rock was crushed into a fine powder using a tungsten-tipped hydraulic ram and a tungsten-carbide ring-mill. Fusion beads for major element analysis were made using a lanthanum oxide flux, and pressed powder pellets were produced for trace element analysis. All samples were analyzed by X-ray fluorescence spectrometry (XRF) using a Philips PW2400 system at the University of Canterbury. Fusion beads and pressed powder elements were irradiated with a rhodium end-window tube operating at 50 kV and 55 mA, and 60 kV and 46 mA, respectively. Standard XRF methods were followed as reported by Weaver *et al.* (1990).

Zircons were separated from ~1 kg samples of fresh rock using standard crushing and heavy-liquid techniques. Zircons were hand picked under a binocular microscope, mounted in epoxy, and polished to reveal mid-sections. Zircons were imaged in a Hitachi SEM for cathodoluminescence (CL). Au-coated zircons were analyzed by SHRIMP-RG (reverse geometry) at the Australian National University, Canberra. U–Th–Pb isotopes were analyzed *in situ* on small areas within single zircon crystals. Data were referenced to the zircon standard TEMORA (Black *et al.*, 2003), which was analyzed repeatedly during the analysis period. Operating procedures used have been described by Muir *et al.* (1997).

Major element compositions of hornblende, plagioclase and biotite from eight samples were determined at Otago University, using a JEOL Superprobe equipped with two wavelength-dispersive spectrometers. An accelerating voltage of 15 kV and a beam current of 12 nA were used, with a beam diameter of 5 μm, and a counting time of ~10 min per spot. To calibrate the major elements, regular checks on various standards of known composition were performed throughout the course of analysis to ensure a relative error of <1%. Computer control and data reduction (ZAF correction procedures) used software by Moran Analytical.

$^{87}Sr/^{86}Sr$ and $^{143}Nd/^{144}Nd$ ratios of 14 samples were measured by multi-collector inductively coupled plasma mass spectrometry (MC-ICPMS) at the Victoria University of Wellington. Samples for Sr isotopic analysis were digested using HF–HNO_3 techniques and Sr was separated using Sr-spec Eichrom resin. Sr mass spectrometric techniques used are a modified version of those described in detail by Waight *et al.* (2002). Samples for Nd isotopic analysis were digested using flux-fusion techniques (Ulfbeck *et al.*, 2003) and Nd was separated using conventional cation exchange and Ln-spec Eichrom resins. Rb/Sr and Sm/Nd ratios were determined by ICP-MS on aliquots of bulk digestions of samples taken prior to chemical separation of Sr and Nd so that age corrections could be carried out. Isotopic ratios were corrected for instrumental mass bias using the exponential law ($^{86}Sr/^{88}Sr = 0{\cdot}1994$; $^{146}Nd/^{144}Nd = 0{\cdot}7219$) and normalized to $^{87}Sr/^{86}Sr = 0{\cdot}710248$ (SRM987) and $^{143}Nd/^{144}Nd = 0{\cdot}5128980$ (BHVO-2). External reproducibility of $^{87}Sr/^{86}Sr$ and $^{143}Nd/^{144}Nd$ ratios is better than ±0·00002.

GEOCHRONOLOGY

To support interpretations made in the field based on the identification of way-up structures, and to determine the precise age and crystallization history of the pluton, U/Pb zircon dating of four samples of the intermediate–felsic host-rocks was undertaken. Figure 6 shows representative CL images of the zircons from the Halfmoon Pluton. The four samples chosen represent different inferred positions within the active magma chamber: AP#G and EC#6C represent leucodiorite host-rock from the inferred base of the chamber, RR#H7 represents a granite host-rock from the middle of the chamber, and TN#29 represents a tonalite host-rock from the inferred top of the chamber. Rims were analyzed to determine the age of crystallization of the zircon within the magma. Several cores were also analysed to ascertain if there was any inheritance within any of the rock samples. All zircons are euhedral to subhedral, and range in length from ~120 to 300 μm, with larger zircons found in rocks from the inferred base of the

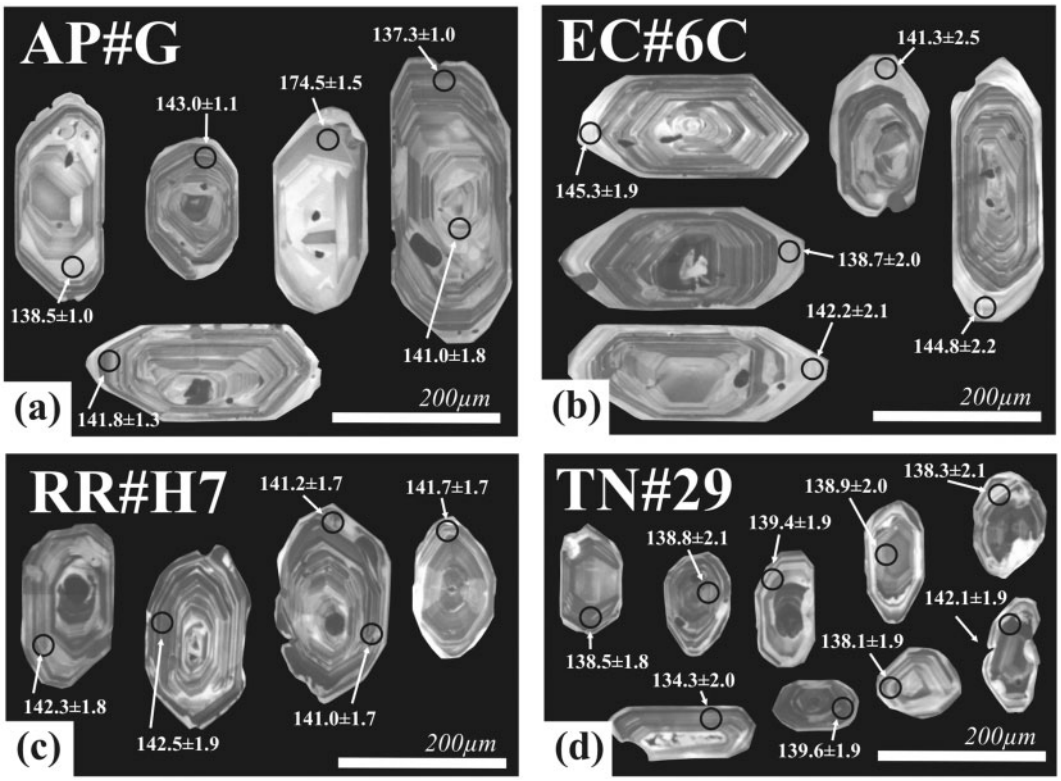

Fig. 6. Cathodoluminescence images of selected zircons from the Halfmoon Pluton. $^{238}U/^{206}Pb$ ages are given in Ma with 2σ errors. Black circles show approximate spot size and location.

chamber (AP, EC), and smaller zircons in rocks from the top of the chamber (RR, TN). Zircon cores all appear to be free of inheritance. Only one anomalously old age was obtained from an Ackers Point zircon (174·6 ± 2·1 Ma), and this is interpreted to have been inherited from the older granitoids through which it intruded. Most zircons exhibit a bright growth rim, although this is more pronounced in the AP and EC zircons than in the rest. These bright rims probably reflect U-poor and REE-rich sections (Corfu *et al.*, 2003). Th/U ratios between 0·2 and 1·7 indicate that these rims are clearly magmatic and not the result of metamorphic overprinting. Narrowly spaced uninterrupted oscillatory zoning is present in all of the zircons, and is consistent with magmatic growth from a melt with a high degree of zircon saturation (Hoskin & Schaltegger, 2003). Zircon morphology and a lack of evidence for inheritance indicate that these zircons represent primary growth solely from the enclosing magmatic system.

Zircon data for the four samples are presented in the form of Tera–Wasserburg concordia diagrams in Fig. 7. The four samples analysed are discussed below in stratigraphic order from the inferred base of the chamber (AP) to the inferred top (TN). Twenty-two zircons were analysed from Ackers Point. Three outliers that showed spurious backgrounds (high Th/U ratios), and were either discordant or were interpreted to represent an older inherited age, were excluded from the age calculations. The remaining 19 analyses have a weighted mean age of 139·4 ± 0·7 Ma (95% confidence) and an MSWD of 1·1 (Fig. 7a). Twenty-seven zircons were analysed from Evening Cove. One discordant outlier was excluded from age calculations, with the remaining 26 analyses giving a weighted mean age of 141·8 ± 1·2 Ma (95% confidence) and an MSWD of 1·16 (Fig. 7b). Twenty zircons were analysed at Ringaringa, 19 of which yield a weighted mean age of 140·1 ± 1·1 Ma (95% confidence) and an MSWD of 1·05 (Fig. 7c). One anomalously old age was excluded from these age calculations. All 26 zircon analyses from The Neck provide a single age population with an age of 138·6 ± 0·7 Ma (95% confidence) and an MSWD of 1·4. CL images show that the zircons from TN#29 do not exhibit the same degree or complexity of zoning as the other three samples discussed above, with faint oscillatory zoning and a lack of any significant bright rim (Fig. 6d).

The ages obtained from the four locations all overlap within 3σ error. The Neck is interpreted to represent a younger adjacent magmatic 'pod', but is still considered part of the same continuously active magmatic system.

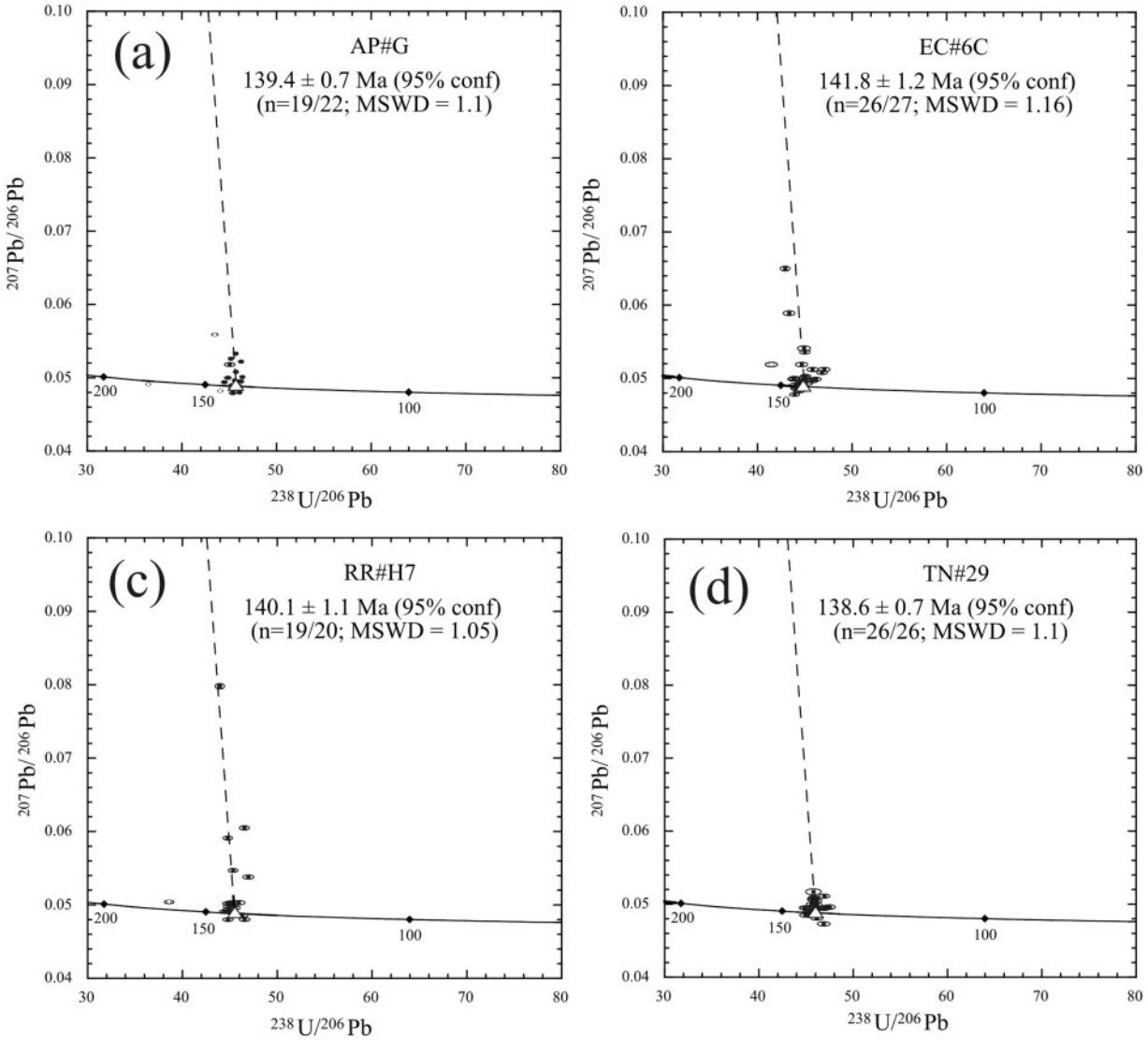

Fig. 7. Tera–Wasserburg U/Pb zircon concordia diagrams. The amount of common Pb in each analysis is inferred from the offset of the point from the concordia along the trajectory of common Pb mixing. Outliers may be caused by inheritance (left of mixing line) or Pb loss (right). Computed $^{238}U/^{206}Pb$ ages are given with 2σ errors.

GEOCHEMISTRY

Whole-rock major and trace element data are plotted on selected Harker variation diagrams in Fig. 8a and b, and versus inferred stratigraphic height in the pluton in Fig. 9. Representative analytical data are reported in Table 2. All rocks from the Halfmoon Pluton define calc-alkaline trends on AFM diagrams, consistent with their generation in an island-arc, subduction-related setting. Classification using the Aluminium Saturation Index (ASI) indicates that the felsic host-rocks towards the top of the chamber (RR and TN) are weakly peraluminous with ASI <1·1, whereas intermediate rocks towards the base of the chamber (AP and EC) are metaluminous. All mafic sheets, enclaves and dikes are metaluminous. An overall trend of large ion lithophile element (LILE) enrichment and high field strength element (HFSE) depletion is evident in all the rocks from the Halfmoon Pluton, characteristic of a subduction signature. Furthermore, an island-arc subduction setting is indicated by depletions in Nb and Ti (McCulloch, 1993).

Intermediate–felsic host-rocks

The major element variation within the intermediate–felsic host-rocks does not follow a simple linear trend from the inferred base of the chamber to the inferred top. SiO_2 compositions range from ~53% at the base of the chamber

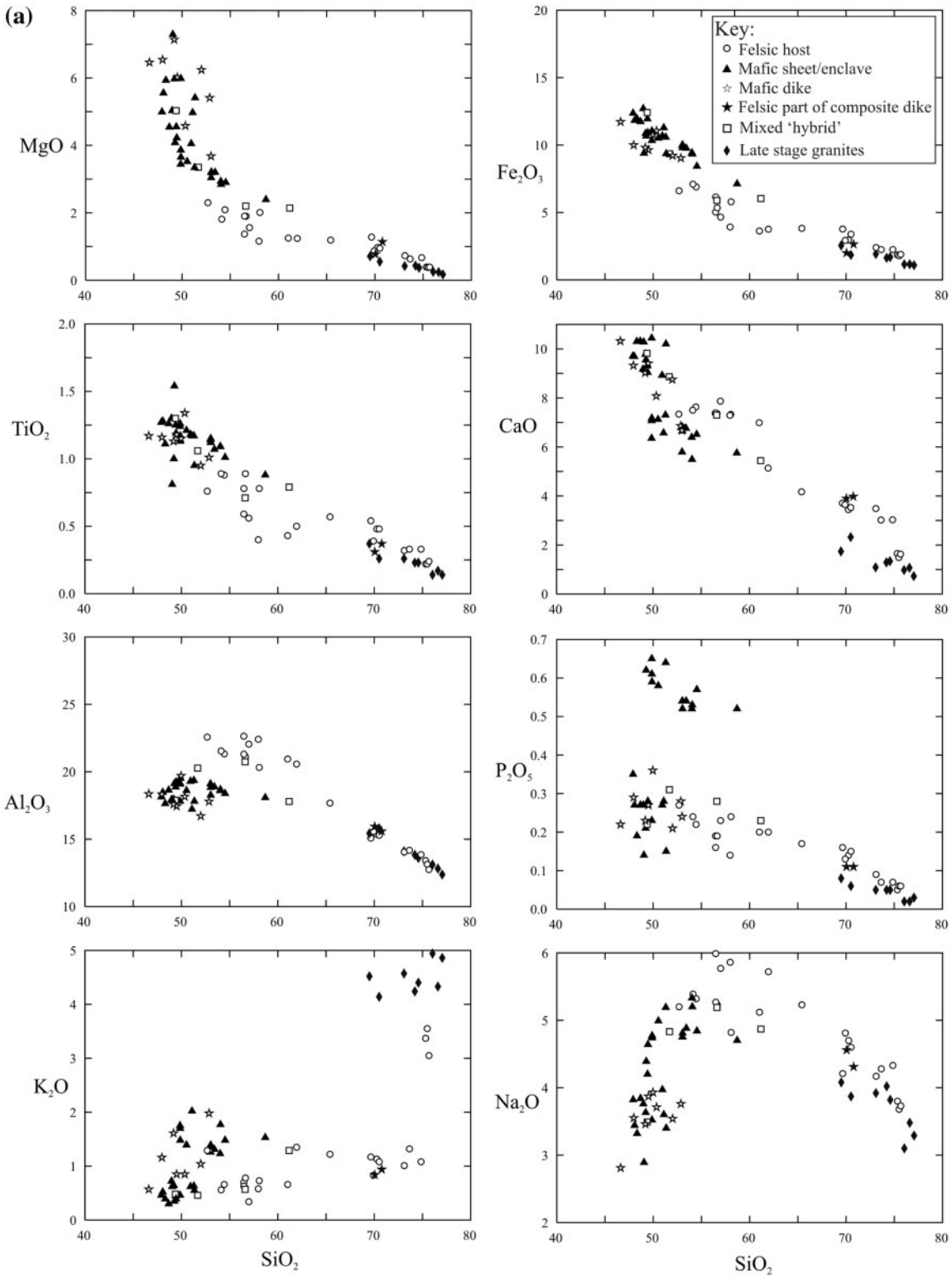

Fig. 8. (a) Whole-rock major-element variation diagrams for the intermediate–felsic host-rocks, the mingled mafic sheets and enclaves, samples of mixed 'hybrid' rock, cross-cutting mafic dikes, the felsic components of composite dikes, and late-stage granites. (b) Selected whole-rock trace-element variation diagrams for the same rocks as plotted in (a). Symbols are the same as those used in (a).

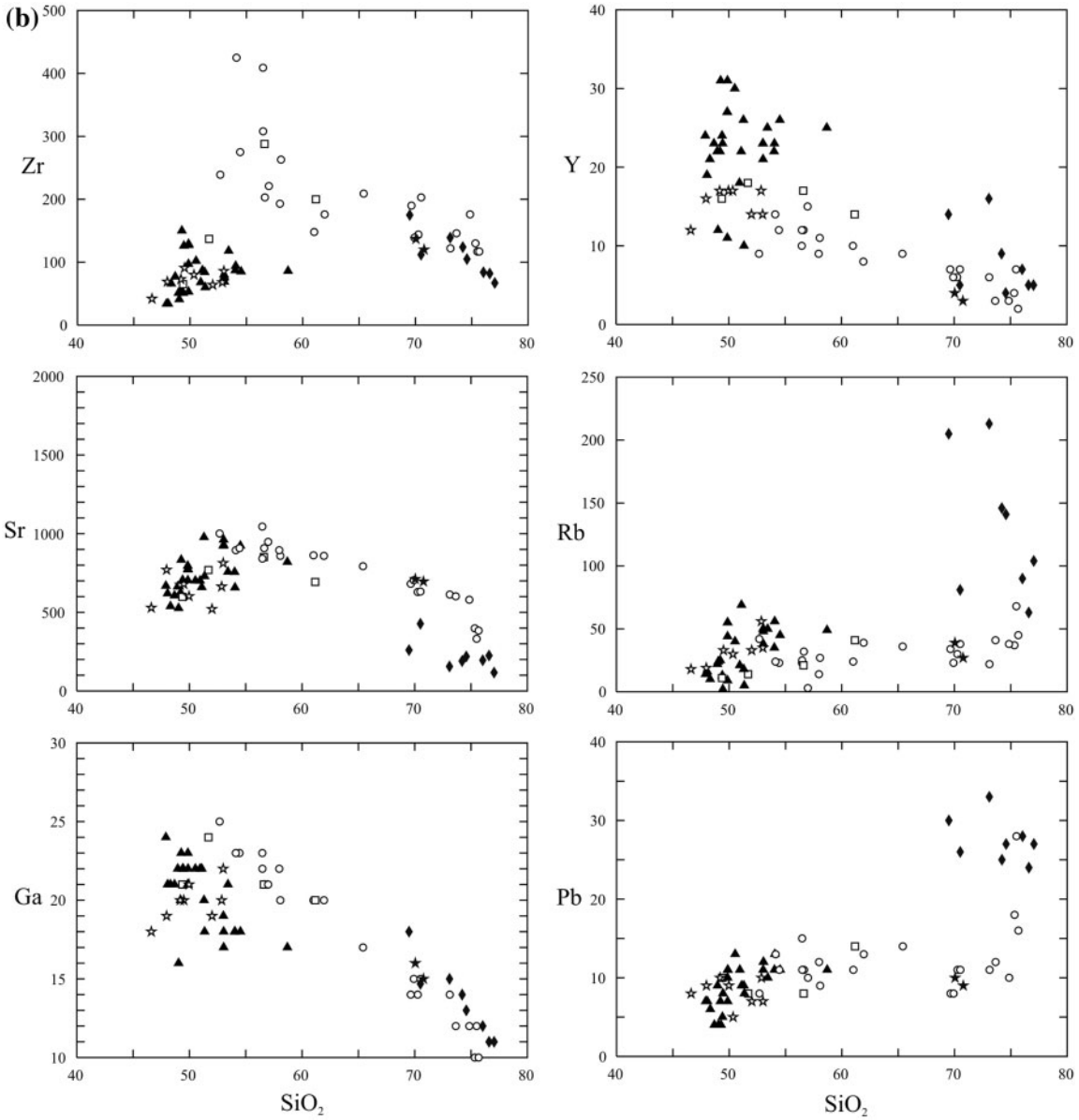

Fig. 8. Continued

(AP) to ~76% at the top (TN) (Fig. 8a). With the exception of K_2O and Na_2O, all other major elements display decreasing concentrations with increasing SiO_2 abundance and inferred height in the sequence. High values of K_2O occur in three of the felsic host samples, which are the only rocks containing alkali feldspar. Al_2O_3 and CaO abundance within the host decreases with increasing height in the chamber. The depletion in Ca and Al, and the concordant rise in K coincide with the mafic phase changing from hornblende to biotite at a higher level in the chamber. Trace element variations within the host-rocks also do not define simple linear trends. Zr, Y, Sr, and Ga show decreases in concentration with increasing SiO_2 content. Pb and Rb concentrations remain constant within the host-rocks, with slightly elevated concentrations in rocks from the inferred top of the chamber. Intermediate host-rocks that display the highest concentrations of Al, Ca and Sr are characterized by large (68–90%) modal percentages of aligned plagioclase.

Variations in the abundance of SiO_2, CaO, Al_2O_3 and Sr within the host-rocks of the Halfmoon Pluton are highlighted in Fig. 9. SiO_2 contents within the host-rocks at the inferred base of the chamber remain relatively constant, ranging between 53 and 63 wt %. SiO_2 increases in

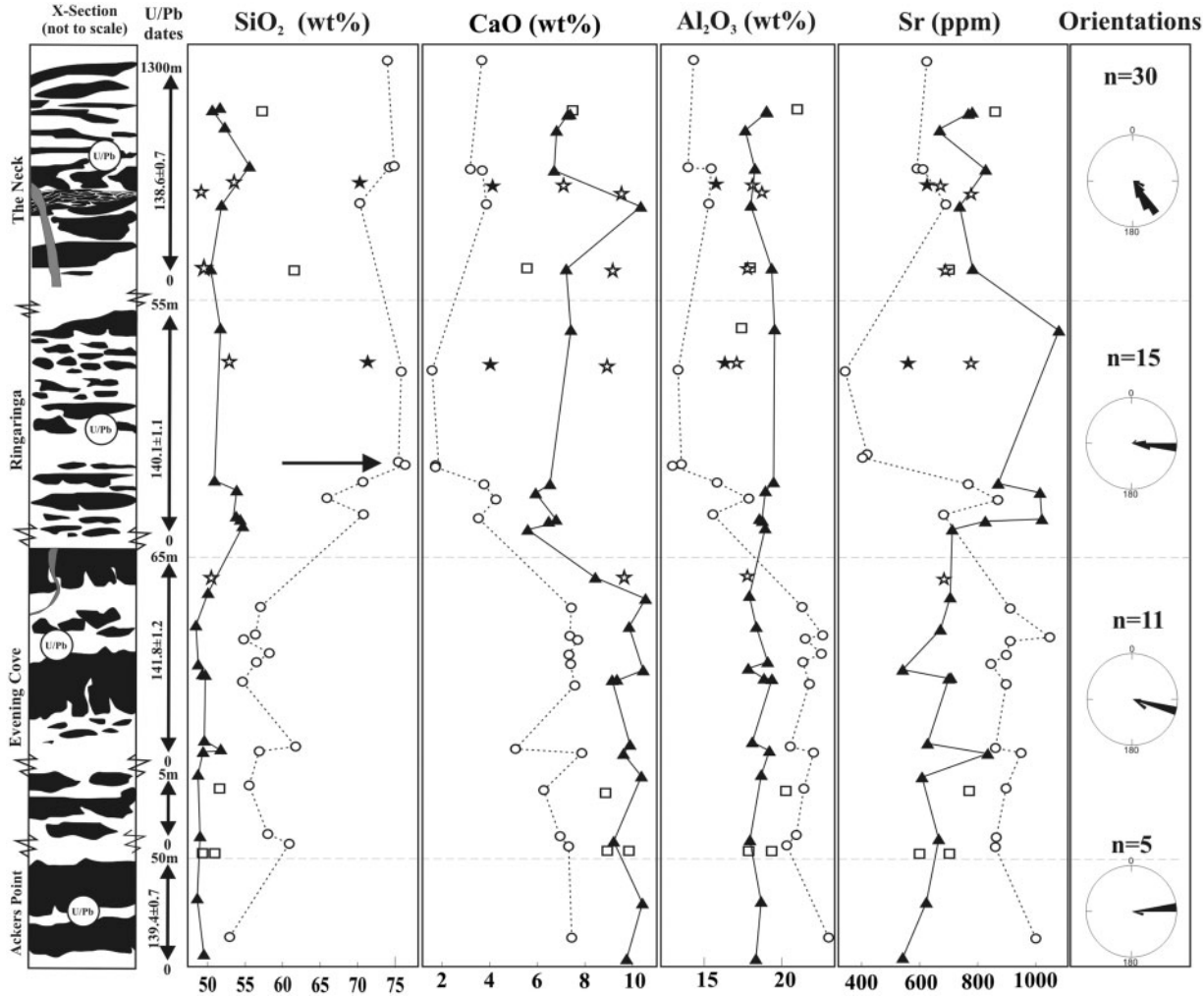

Fig. 9. Geochemical variations vs stratigraphic height. Symbols are the same as those used in Figure 8. SiO_2 content within the felsic rocks increases with increasing height in the chamber, whereas the SiO_2 content in the mafic rocks remains constant. CaO contents within both the mafic and felsic rocks mimic each other, with a decrease in CaO with increasing height in the chamber. Al_2O_3 contents within the felsic rocks decrease with increasing height, whereas the Al_2O_3 content in the mafic rocks remains constant. TiO_2 contents within both rocks show a slight decrease from the base to the top. Sr concentrations within the host decrease substantially towards the top of the chamber, and increase slightly in the mafic rocks. Arrow indicates the incoming of alkali feldspar and muscovite at ~75% SiO_2. n, number of mafic sheets and enclave orientations measured.

abundance in the host-rocks from Ringaringa and The Neck, ranging between 65 and 79 wt %. The concentrations of Al_2O_3, CaO and Sr show reverse trends to that of SiO_2, with felsic rocks at The Neck and Ringaringa being depleted in Ca, Al, and Sr relative to those at Evening Cove and Ackers Point (Fig. 9). Sr concentrations at The Neck are, however, slightly more elevated than those at Ringaringa.

Mafic sheets and enclaves

Mafic sheets and enclaves throughout the chamber have restricted SiO_2 contents, ranging from 48% at the base to 55% at the top. Major element trends are not as well defined as those for the felsic host; however, most show trends of decreasing concentrations with increasing SiO_2 and stratigraphic height in the chamber. Na_2O concentrations increase with increasing SiO_2 until ~52% SiO_2; thereafter Na_2O decreases. This is correlated with a change in the composition of the plagioclase crystallizing, which becomes less Ca-rich and more Na-rich with higher SiO_2 contents. Al_2O_3 concentration remains uniform throughout the sequence. Two distinct clusters are observed in the P_2O_5 concentrations, both of which decrease with increasing SiO_2. Zr, Sr, Rb and Pb concentrations increase with increasing SiO_2, whereas Ga concentrations decrease. A scattered trend is observed with Y. Mafic enclaves from

Table 2: Representative major and trace element compositions of plutonic rocks from the Halfmoon Pluton

Rock type:	Mingled mafic rocks									Composite dike			
Details:	Sheet	Sheet	Sheet	Sheet	Sheet	Sheet	Enclave	Enclave	Enclave	Felsic	Mafic	Felsic	Mafic
Sample:	EC#10 M	EC#B4	EC#6 M	TN#37	TN#8	AP#M	RR#K1m	RR#M2	TN#6	RR#FDf	RR#FDm	TN#24f	TN#24m
SiO_2	49·87	49·22	48·32	54·53	58·70	48·07	49·86	54·05	49·88	70·05	52·01	70·78	52·87
TiO_2	1·13	1·00	1·11	1·01	0·88	1·28	1·24	1·09	1·17	0·31	0·95	0·37	1·01
Al_2O_3	17·81	17·95	17·64	18·38	18·08	18·47	19·08	18·67	19·50	15·94	16·72	15·59	17·79
Fe_2O_3	10·33	10·86	11·94	8·42	7·12	11·82	10·93	9·33	10·95	2·00	9·22	2·65	9·03
MnO	0·15	0·21	0·22	0·18	0·14	0·18	0·22	0·17	0·20	0·02	0·17	0·03	0·13
MgO	5·98	5·97	5·93	2·90	2·39	5·55	3·44	2·84	3·65	0·77	6·24	1·14	5·41
CaO	10·44	9·78	10·30	6·51	5·75	9·69	6·35	5·49	7·17	3·90	8·75	3·98	6·86
Na_2O	3·52	3·63	3·32	4·84	4·70	3·44	4·74	5·20	4·77	4·56	3·54	4·31	3·76
K_2O	0·46	0·64	0·39	1·48	1·53	0·52	1·75	1·77	1·48	0·84	1·04	0·94	1·98
P_2O_5	0·23	0·21	0·19	0·57	0·52	0·27	0·65	0·53	0·59	0·11	0·21	0·11	0·28
LOI	0·19	0·61	0·66	0·45	0·56	0·91	0·79	0·95	0·57	0·24	1·34	0·10	0·38
Total	100·10	100·08	100·01	99·26	100·37	100·21	99·09	100·10	99·92	98·74	100·19	99·99	99·50
Ba	180	155	134	451	571	187	798	1084	721	434	259	371	627
Rb	9	25	10	45	49	16	55	56	55	39	33	27	56
Sr	703	625	538	923	820	619	795	657	771	712	521	696	663
Pb	7	7	6	11	11	7	10	13	11	10	7	9	10
Zr	53	56	66	85	86	34	97	94	127	137	64	120	68
Nb	3	3	3	5	4	4	4	3	4	3	3	3	4
Y	11	22	21	26	25	19	27	23	31	4	14	3	17
V	338	283	347	53	43	385	89	75	142	34	239	51	219
Cr	103	94	35	—	—	73	—	—	—	—	276	7	52
Ni	23	17	16	—	—	20	—	—	—	5	58	12	67
Zn	93	114	114	76	67	101	108	92	122	21	95	27	96
La	—	—	—	17	9	—	16	16	11	21	8	15	12
Ce	27	24	25	40	33	20	65	35	42	42	27	25	49
Nd	18	18	—	18	15	18	25	23	18	<10	23	<10	<10
Ga	21	20	21	18	17	21	21	18	22	16	19	15	20

(Continued)

Table 2: Continued

Rock type:	Felsic host								Mafic dike		Later granite			
Details:														
Sample:	EC#9H	EC#6C	EC#3g	RR#H1	RR#H6	TN#35	TN#31	AP#G	TN#12	EC#10D	BB#G2	UI#G1	FP#G1	LB#G1
SiO_2	56·64	57·98	61·94	65·41	75·67	73·65	70·51	52·68	50·35	49·51	69·50	76·60	77·05	70·51
TiO_2	0·89	0·40	0·50	0·57	0·24	0·33	0·48	0·76	1·34	1·18	0·37	0·17	0·14	0·26
Al_2O_3	21·11	22·41	20·57	17·68	12·75	14·18	15·29	22·57	18·16	17·45	15·43	12·82	12·38	15·80
Fe_2O_3	5·34	3·92	3·76	3·82	1·89	2·25	3·39	6·61	11·06	9·63	2·55	1·16	1·09	1·85
MnO	0·08	0·05	0·05	0·06	0·02	0·03	0·04	0·07	0·14	0·16	0·04	0·01	0·02	0·02
MgO	1·90	1·16	1·24	1·19	0·39	0·63	0·95	2·30	4·58	6·02	0·71	0·24	0·17	0·55
CaO	7·36	7·29	5·14	4·17	1·63	3·02	3·53	7·34	8·08	9·41	1·74	1·07	0·73	2·32
Na_2O	5·23	5·86	5·72	5·23	3·73	4·28	4·60	5·20	3·71	3·87	4·08	3·48	3·29	3·87
K_2O	0·78	0·58	1·35	1·22	3·05	1·32	1·08	1·29	0·85	0·85	4·52	4·33	4·86	4·14
P_2O_5	0·19	0·14	0·20	0·17	0·06	0·07	0·15	0·27	0·37	0·27	0·08	0·02	0·03	0·06
LOI	0·69	0·48	−0·19	0·57	0·42	−0·20	0·47	0·56	1·81	1·74	1·13	0·37	0·42	0·57
Total	100·21	100·27	100·29	100·10	99·84	99·55	100·48	99·65	100·44	100·09	100·15	100·28	100·17	99·95
Ba	389	273	679	614	2940	556	524	697	361	293	529	1225	522	1486
Rb	32	14	39	36	45	41	38	42	30	33	205	63	104	81
Sr	908	895	859	793	384	602	632	1001	715	679	260	225	117	427
Pb	11	12	13	14	16	12	11	8	5	11	30	24	27	26
Zr	203	193	176	209	117	146	203	239	80	91	175	82	67	112
Nb	3	2	3	2	—	3	3	3	3	4	4	—	—	3
Y	12	9	8	9	2	3	7	9	17	17	14	5	5	5
V	127	85	55	41	15	21	35	131	327	285	42	14	12	35
Cr	6	5	—	—	—	—	—	8	18	238	—	—	4	—
Ni	—	4	—	—	4	4	3	6	11	37	5	—	—	5
Zn	57	38	47	38	16	22	33	72	84	91	37	12	16	24
La	8	15	7	14	13	24	18	13	—	—	24	8	10	19
Ce	23	36	27	20	21	39	36	35	22	31	43	13	16	49
Nd	—	—	—	—	—	20	—	21	19	27	18	—	—	—
Ga	21	22	20	17	10	12	15	25	22	20	18	11	11	15

Data are normalized to 100% anhydrous. Major elements are given in wt % and trace elements in ppm. Loss on ignition (LOI) values were calculated by weight difference. —, values below the detection limit.

RR and TN are all enriched in Na_2O, K_2O, P_2O_5 (the upper cluster of data), Ce, Y, Rb and Ba relative to mafic sheets from AP, EC and TN. These enriched enclaves also have higher modal abundances of apatite (between 1 and 2%) and biotite. Variations in the abundance of SiO_2, CaO, Al_2O_3 and Sr within the mafic rocks of the Halfmoon Pluton are highlighted in Fig. 9. SiO_2 and Al_2O_3 concentrations remain uniform throughout the sequence. Variations in CaO concentration appear to mimic those in the surrounding host-rock. Sr concentrations remain relatively constant throughout the sequence although they are slightly elevated at Ringaringa. Samples which were classified as 'mixed' or 'hybrid' rocks in the field (i.e. where a mafic sheet or enclave had physically mixed by exchanging crystals with the surrounding host) also show hybrid chemistry, plotting intermediate to the associated mafic and felsic components (Fig. 9).

As indicated in Fig. 9, the compositional contrast between the two interacting magmas with respect to SiO_2 was initially small, with the host-rock ranging between ~53 and 62 wt % SiO_2, and the mingled mafic rocks ranging between 49 and 51 wt % SiO_2 at Ackers Point and Evening Cove. With increasing height in the chamber and a move towards more felsic host-rock compositions, this compositional gap becomes much greater. A large change occurs at Ringaringa, where the composition of the host changes from 65 wt % to >75 wt % SiO_2. Mafic sheets and enclaves within this section have an average SiO_2 composition of 55%. The composition of the host-rock from this point appears to remain relatively constant, with felsic host-rocks at The Neck ranging between 70 and 75 wt % SiO_2, and mafic rock compositions ranging between 50 and 55 wt % SiO_2.

Mafic, composite and felsic dikes

Mafic dikes and the mafic components of composite dikes are chemically indistinguishable from the mafic sheets and enclaves, suggesting that they originate from the same relatively primitive magma source. The felsic component of the composite dikes is compositionally identical to the felsic host-rock they intrude. This felsic material is different in composition from the late-stage granite dikes and larger granite intrusions, which are highly silicic, with high SiO_2 contents ranging between 70 and 80%. The later granitic intrusions are enriched in K_2O and Pb relative to the rest of the Halfmoon Pluton, with ~4·5 wt % K_2O compared with <1·5 wt % for almost all of the intermediate–felsic host samples, and ~27 ppm Pb compared with <18 ppm Pb for all of the host-rocks. These granitic dikes and larger intrusive bodies represent later cross-cutting magmas that intruded the Halfmoon Pluton after it was completely crystallized.

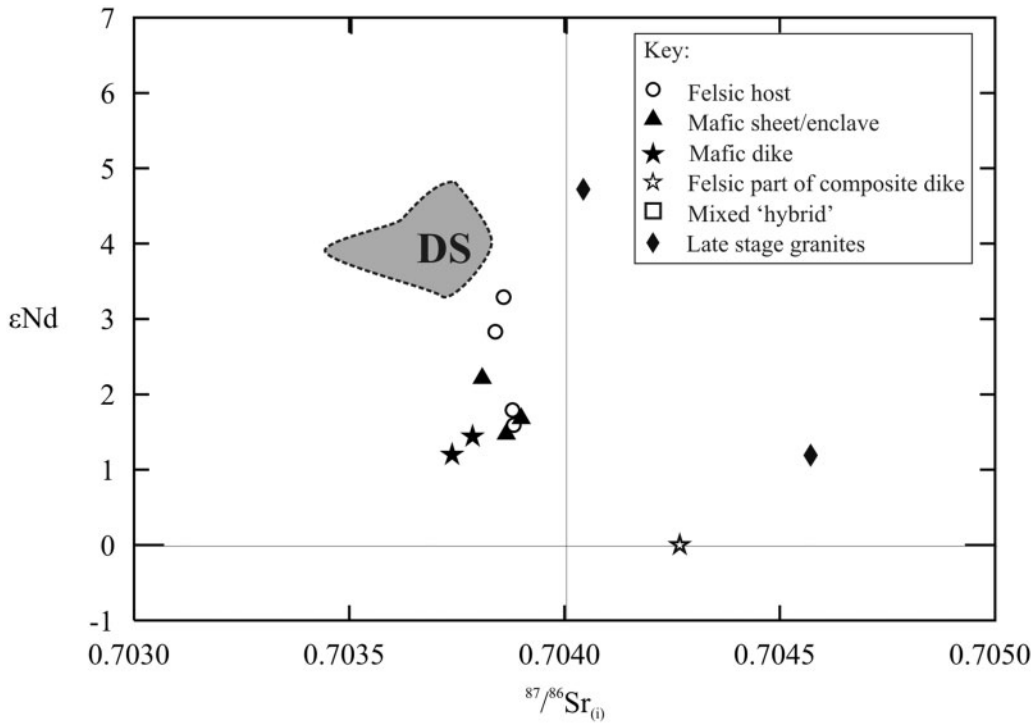

Fig. 10. ε_{Nd}(140 Ma) vs initial $^{87}Sr/^{86}Sr$ for the Halfmoon Pluton and cross-cutting granite sheets. Darran Suite field (DS) from Muir *et al.* (1998)

Table 3: Sr and Nd isotopic data from rocks of the Halfmoon Pluton

Sample	Type	Sr (ppm)	Rb ^{86}Sr	$^{87}Rb/^{86}Sr_{(m)}$	$^{87}Sr/^{86}Sr_{(i)}$	$^{87}Sr/^{144}Nd$	$^{147}Sm/^{144}Nd$	$^{143}Nd/$	$\varepsilon_{Nd}(T)$
AP#G	Diorite host	1001	42	0·045	0·704140	0·703879	0·207	0·512739	1·97
AP#M	Mafic sheet	619	16	0·015	0·703964	0·703879	0·238	0·512753	2·25
EC#6C	Diorite host	895	14	0·019	0·703966	0·703859	0·210	0·512819	3·53
EC#6 M	Mafic sheet	538	10	0·005	0·703835	0·703809	0·258	0·512807	3·30
RR#H6	Host granite	384	45	0·097	0·704443	0·703882	0·106	0·512720	1·59
TN#35	Tonalite host	602	41	0·056	0·704162	0·703839	0·144	0·512734	1·88
TN#37	Mafic enclave	923	45	0·053	0·704189	0·703884	0·223	0·512746	2·12
TN#24m	Mafic comp dike	663	56	0·089	0·704254	0·703739	0·133	0·512699	1·20
TN#24f	Felsic comp dike	696	27	0·040	0·704495	0·704268	0·095	0·512638	0·00
LB#G1	Granite (later?)	427	81	0·178	0·705053	0·704044	0·215	0·512896	5·04
BB#G2	Granite (later)	260	205	0·770	0·708941	0·704572	0·213	0·512714	1·47
TN#26	Mafic dike	675	42	0·067	0·704171	0·703787	0·241	0·512752	2·23

For ε_{Nd} calculations, $^{143}Nd/^{144}Nd$ CHUR = 0·512638; $^{147}Sm/^{144}Nd$ CHUR = 0·1967.

Sr–Nd isotopes

$^{87}Sr/^{86}Sr$ and $^{143}Nd/^{144}Nd$ data for 14 selected samples from the Halfmoon Pluton are plotted in Fig. 10 and listed in Table 3. Initial $^{87}Sr/^{86}Sr$ values for all felsic host, mafic sheets and enclaves, composite dikes and mafic dikes occupy a very restricted range between 0·70379 and 0·70427. ε_{Nd} values display a slightly less restricted range, between +3·5 and +1·9. No significant crustal component can be inferred from the isotopic signature; however, melting of young primitive oceanic crust cannot be ruled out. The limited variation in initial isotopic compositions can be ascribed to small variations in mantle and crustal components such as aqueous fluids derived from the subducted slab, and minor crustal contamination. Another possible explanation for the limited strontium isotope ratios and spread of neodymium isotope ratios is diffusive exchange between more and less primitive materials at depth, either contrasting rocks in the source region or mafic and felsic magmas during ascent (Bachl *et al.*, 2001). The Halfmoon Pluton rocks display primitive initial ratios, consistent with only a limited interval between the time of extraction from the mantle and crystallization. The isotopic values confirm that the mingled mafic and felsic rocks are genetically related, originating from the same primitive source, which is depleted relative to Bulk Earth. The field for plutonic rocks from the Darran Suite (Muir *et al.*, 1998) is also plotted in Fig. 10, and indicates that the Halfmoon Pluton has a slightly more evolved isotopic signature.

Two samples from later cross-cutting granite bodies have slightly more elevated initial $^{87}Sr/^{86}Sr$ values of 0·70404 and 0·70457, and ε_{Nd} values of +5·0 and +1·5 respectively. These granites are interpreted as having been derived from a distinct source with a more fractionated composition and involving some degree of crustal contamination. They are not petrogenetically related in any simple way to the Halfmoon Pluton rocks. As discussed above, the felsic component of the composite dikes that cross-cut the chamber has similar whole-rock compositions to the host-rocks that enclose them; however, the Sr–Nd isotopic signature of the only sample analyzed is more comparable with the later cross-cutting granites. This felsic material may therefore represent granitic dikes from a more evolved source, which was subsequently incorporated into a composite dike along with the intruding mafic magma; however, it is hard to be certain based on the limited dataset.

Some workers have suggested that complete isotopic equilibrium between coeval mafic and felsic magmas can occur, with mafic enclaves equilibrating with the surrounding felsic host (Barbarin & Didier, 1992; Poli *et al.*, 1996; Waight *et al.*, 2001). Chemical and isotopic equilibrium has generally been proposed within plutons that contain small quantities of mafic enclaves, whereby there is a larger effect of the felsic host on the enclosed mafic enclaves. Chemical exchange and isotopic equilibration of the mafic rocks is likely to have been obstructed by the quickly formed fine-grained quenched margins on the mafic sheets and enclaves. These chilled margins stop the mechanical transfer of mass and crystals between the two magmas, and probably inhibit chemical exchange and therefore isotopic equilibration (Barbarin & Didier, 1992). Chemical and isotopic equilibration of the host is also unlikely, as the composition of the enclosed mafic rocks does not mimic that of the intermediate–felsic host (Fig. 8). Rapid crystallization of the mafic magma would result in

Table 4: Pressure and temperature estimates of rocks from the Halfmoon Pluton

Sample	Rock type	An%	*P* (kbar)*	Depth (km)*	*T* (°C)†	*P* (kbar)‡	Depth (km)‡	*T* (°C)‡
AP#G	Felsic host	37	2·7	9·5	722	1·2	4·2	805
EC1/6	Felsic host	38	2·8	9·8	724	1·4	4·9	812
EC#6	Felsic host	40	2·6	9·1	753	1·4	4·9	819
EC#9H	Felsic host	41	2·4	8·4	738	1·2	4·2	814
TN#22	Felsic host	38	2·3	8·1	729	1·2	4·2	807
TN#30	Mafic enclave	30	2·8	9·8	723	1·3	4·6	807
TN#17	Composite dike	39	2·5	8·8	706	1·1	3·9	794

*Pressures and corresponding depths of crystallization calculated using the Al-in-hornblende geobarometer of Anderson & Smith (1995).
†Temperatures calculated using the Holland & Blundy (1994) plagioclase geothermometer. Calculation depths are based on 1 kbar being equivalent to 3·5 km of crust.
‡Pressures and corresponding depths and temperatures calculated using the amphibole thermobarometer of Ridolfi *et al.* (2010).

the formation of a fine-grained quenched margin, therefore limiting any significant chemical or isotopic diffusion (Sparks & Marshall, 1986). The isotopic similarity between the mafic and intermediate–felsic rocks of the Halfmoon Pluton is therefore interpreted to indicate that the magmas are consanguineous, and followed evolutionary trends from the same primary liquid with only minor chemical modification through interaction with other mantle or crustal components.

PRESSURE–TEMPERATURE ESTIMATES

Estimates of crystallization pressures and equivalent depths were made using amphibole compositions obtained by electron microprobe. Initial field observations regarding the emplacement depths of plutons (Hammarstrom & Zen, 1986) and subsequent experimental studies have shown that the total Al content of amphibole is a function of both temperature and pressure (Johnson & Rutherford, 1989; Blundy & Holland, 1990; Thomas & Ernst, 1990; Schmidt, 1992; Anderson & Smith, 1995). Pressure estimates for Halfmoon Pluton amphiboles were calculated using the temperature-corrected Anderson & Smith (1995) geobarometer; these are summarized in Table 4. Application of this technique requires the presence of the appropriate buffering assemblage of hornblende, plagioclase, orthoclase, biotite, quartz, Fe–Ti oxide (magnetite or ilmenite), apatite, titanite plus melt and a fluid phase. Almost all samples within the Halfmoon Pluton are too mafic to contain orthoclase; however, Hollister *et al.* (1987) have suggested that the absence of orthoclase would result in pressure overestimates, perhaps as high as 1 kbar. Therefore, the results presented in Table 4 represent maximum pressures and depths of emplacement for the Halfmoon Pluton.

Calculated pressures range between 2·3 and 2·8 kbar, which correspond to crystallization depths of between 8·1 and 9·8 km, respectively. Associated errors on the pressure calculations are ±0·6 kbar, suggesting that all the analyzed samples from within the Halfmoon Pluton crystallized at pressures between ~1·7 and 3·4 kbar (equating to 6·3 and 13·3 km, respectively). Because crystallization of the magma must be well advanced to produce the entire mineral assemblage required for the Al-in-hornblende barometer, such plutons are likely to be largely solidified and the calculated pressures probably represent the conditions during final emplacement (Leake & Said, 1994). Furthermore, uncertainty still exists as to the mineral assemblage that was actually crystallizing at the time hornblende was crystallizing. Interpretations regarding actual emplacement depths using the Al-in-hornblende geobarometer are therefore not well constrained. Quantification of actual emplacement depths is challenging; however, the presence of amygdules within mafic enclaves at The Neck (inferred top of the chamber) suggests much shallower depths of crystallization than those obtained using the Al-in-hornblende geobarometer.

Pressure estimates were also made using the new thermobarometric formulations of Ridolfi *et al.* (2010), which are reported in Table 3. These new formulations have currently been applied only to volcanic and experimental amphiboles, and therefore caution needs to be exercised in interpreting the results. This method uses an entirely empirical approach, linking thermobarometric equations exclusively to amphibole composition. Application of this

method requires the amphibole to have a composition of Al-number $\leq 0{\cdot}21$ [Al-number $= Al_{vi}/(Al_{vi} + Al_{iv})$] and $Mg/(Mg + Fe^{2+}) > 0{\cdot}5$, and for the amphiboles to have crystallized from calc-alkaline magmas. Halfmoon Pluton amphiboles have Al-number ranging between 0·04 and 0·18 and $Mg/(Mg + Fe^{2+})$ ranging between 0·59 and 0·74, and are from rocks with calc-alkaline geochemistry, and therefore fit the suggested criteria for application of this new method. Calculated pressures range from ~1·1 to ~1·4 ± 0·3 kbar, with corresponding depths of 3·9–4·9 km. These depths are significantly lower than the depth estimates calculated using the Al-in-hornblende geobarometer; however, they appear more consistent with the shallower emplacement depths indicated by the presence of amygdules. All estimated pressures from both methods overlap within error, and therefore what can be concluded from these results is that the rocks within the Halfmoon Pluton were emplaced and crystallized in the upper crust within a single composite pluton. The Halfmoon Pluton intrudes into ~5 Myr older volcanic rocks to the south, consistent with upper crustal depths of emplacement.

Temperature estimates based on the hornblende–plagioclase geothermometer of Holland & Blundy (1994) give temperatures ranging from 706–753°C; however, with geothermometer uncertainties of ±75°C, the calculated temperature differences overlap and are therefore not significant. Temperature estimates based on the thermobarometric equations of Ridolfi *et al.* (2010) give higher temperatures than the plagioclase–hornblende geothermometer, with temperatures ranging from 794 to 819°C and corresponding uncertainties of ±22°C. These higher temperatures are probably more accurate than the lower temperature estimates, which fall close to the lower stability field of hornblende in coexistence with biotite, plagioclase, quartz and liquid (Deer *et al.*, 1997).

IDENTIFICATION OF MAGMATIC PROCESSES

The magmatic processes that operated within the Halfmoon Pluton can be interpreted from the structures and textures preserved in the mingled magmas, field and petrographic evidence, and geochemical data. Identification of these processes provides clues to the processes that operate within active island-arc settings.

Magma mingling and mixing

As established from field observations, magma mingling is the dominant physical interaction process occurring within the Halfmoon Pluton. Mingling styles vary according to position within the chamber, and are likely to have been caused by a number of factors. Fluid dynamic studies (Campbell & Turner, 1985; Snyder & Tait, 1995) show that the main parameters that favour mingling rather than mixing are compositional contrast, the relative volumes of the two magmas, the rate of replenishment, volatile content, and most importantly contrasts in temperature and degree of crystallization (and therefore density).

The interacting magmas within the Halfmoon Pluton have been shown to be very similar in composition towards the base of the chamber (AP and EC), especially with respect to SiO_2, with mafic rocks between 48 and 51% SiO_2, and host-rocks between 53 and 60% SiO_2. The compositional contrast between the mafic and felsic magmas becomes much greater towards the top of the chamber (RR and TN), with mafic rocks between 52 and 55% SiO_2, and felsic host-rocks between 66 and 75% SiO_2. This change in compositional contrast coincides with a change in mingling style from mafic sheet formation to mafic enclave formation. Comparison with well-studied plutons that exhibit large compositional contrasts (Wiebe, 1993*a*; Wiebe *et al.*, 200l; Miller & Miller, 2002; Harper *et al.*, 2004; Collins *et al.*, 2006), however, reveals that the mingling structures and textures observed within the Halfmoon Pluton are also found within these plutons. Contrast in composition is therefore not envisaged to have played a major role in the mingling style preserved.

In any magma interaction relationship, the relative volumes of the two interacting materials play an important role. If there is a large influx of mafic magma there may be an insufficient quantity of cooler felsic host magma to chill against, and therefore mixing is preferred. Alternatively, when very small amounts of mafic magma are injected into large quantities of felsic magma, mingling more readily occurs and mafic enclave formation may be favoured. In the case of the mingling structures observed at Ringaringa, the presence of mafic enclave swarms within larger volumes of felsic host than anywhere else within the sequence suggests that smaller volumes of mafic magma were injected, promoting mafic enclave formation.

Temperature contrast and degree of crystallinity of the two interacting magmas are the key factors controlling the style of magma mingling. Without a sufficient temperature contrast, rapid chilling of the mafic magma against the cooler felsic magma will not occur, and therefore mixing will be favoured. The degree of crystallization of the felsic host is a function of temperature; liquid-rich magmas will be too hot for mingling to occur, whereas liquid-poor magmas are too crystalline to permit mingling. Mafic sheets and enclaves within the Halfmoon Pluton have fine-grained chilled margins, and coarser-grained centres, indicating that the mafic magma was much hotter than the felsic host magma it chilled against. Thermal equilibration between the felsic host and the injecting mafic magma would have occurred relatively quickly as a result of the rapid quenching of the mafic magma (Blundy & Sparks, 1992). Rapid crystallization of the mafic magma is also indicated by the presence of

bladed biotite and acicular apatite within the mafic sheets and enclaves. Temperature and crystallinity contrasts and, therefore, relative rheological contrasts between the two magmas play the most significant role in inhibiting mixing between the two magmas.

Mechanical mixing is also common throughout the chamber, with physically mixed mafic enclaves often occurring next to non-mixed mafic enclaves. Mixing is evident by the presence of plagioclase and quartz xenocrysts within the mafic enclaves as a result of the physical exchange of crystals between the host and the mafic enclave. Mixing between the two interacting magmas can occur at four locations: prior to emplacement, during emplacement as a result of flow-front instabilities, at the base of mafic sheets, and at the top of the mafic sheet at the contact with the overlying felsic host (Wiebe *et al.*, 2002). Most mafic enclaves within the Halfmoon Pluton appear to have undergone localized mechanical mixing with the intermediate–felsic host, and are therefore likely to have had lower contrasts in temperature with the adjacent host. Enclaves that occur in locations where there is evidence for vigorous flow within the chamber also commonly display gradational, mixed contacts with the host. Localized magma mixing involves the mechanical exchange of plagioclase and quartz crystals from the felsic host to the mafic inclusions, and gradational contacts between the mafic and felsic rocks. Mixing also occurs on a large scale, with whole enclave swarms displaying evidence for physical mixing with the host. Mixing within these enclave swarms may have occurred within composite synplutonic dikes, which then flowed into location as horizontal swarms. At The Neck, mixing either prior to or during emplacement has resulted in the formation of 'composite' enclaves, which mixed elsewhere within the chamber before being transported to their current locations. These composite enclaves have cuspate, quenched, mingled contacts with the adjacent felsic host-rocks, indicating that they were relatively soft or mushy when they were emplaced at their current location (Fig. 3b).

Crystal accumulation, compaction and magmatic flow

Foliations in plutonic bodies may develop as a result of several processes including, but not limited to, tectonic stress and deformation, magmatic flow, compaction and crystal settling. All field and petrographic evidence suggests that the structural and textural features preserved in the Halfmoon Pluton rocks were the result of magmatic processes and not solid-state deformation. Where quartz is present, it shows little to no sign of plastic deformation associated with solid-state deformation.

Foliation within the mafic rocks is defined by mafic sheet orientation and aligned mafic enclaves showing a common elongation direction between 90° and 110° (Figs 1 and 9). The consistent orientation of mafic sheets and enclaves throughout the chamber (except for The Neck—see next section) is interpreted to represent the original orientation at which the mafic magmas were injected and flowed between the lower crystal-rich mush and the upper crystal-poor host magma. Mafic enclave swarms commonly display structures indicating that they were affected by magmatic flow, including the orientation of small mafic enclaves around large mafic enclaves that appear to have acted as barriers to flow within the chamber. Mineral foliation in the surrounding host-rocks parallels that of the mafic enclave orientation where there is evidence for magmatic flow.

Magmatic foliations within the intermediate–felsic host-rocks are typically oriented parallel to the direction of mafic sheet and enclave orientation. Foliation within the host-rocks is defined by the orientation of euhedral tabular plagioclase crystals, which is strongest towards the inferred base of the chamber. Large tabular plagioclase crystals make up >85% of the leucodiorite host-rocks at AP and EC, and are aligned, along with euhedral hornblende and sometimes biotite, and separated by small amounts (<5%) of interstitial quartz. Although magmatic flow appears responsible for some of the mineral alignment present in the host-rocks, crystal accumulation is probably responsible for the strong crystal alignment observed in the host-rocks towards the base of the chamber. The occurrence of granite cumulates is considered by many to be unlikely because of the high viscosities of felsic melts, which would inhibit the sinking and accumulation of crystals (Harper *et al.*, 2004). However, recent viscosity measurements have shown that crystals within a hydrous felsic magma at temperatures of 750–800°C may settle at rates of >1 m/year, which would be sufficient for crystal accumulation to occur (Baker, 1996; Scaillet *et al*, 1998). A number of both composite and homogeneous plutons exhibit compelling field and geochemical evidence supporting downward crystal accumulation (Wiebe & Collins, 1998; Bachl *et al.*, 2001; Collins *et al.*, 2006; Kamiyama *et al.*, 2007). The identification of cumulates within the Halfmoon Pluton is further supported by geochemical evidence.

The host-rocks at AP and EC, which display strong crystal alignment, have higher concentrations of Al_2O_3, CaO and Sr than the host-rocks towards the top of the chamber (RR and TN), which do not display cumulate textures. High Zr contents also occur within host-rock samples at AP and EC, and are interpreted to result from the accumulation of zircon. Rocks with SiO_2 concentrations as low as those at EC and AP (<60 wt %) would not normally exhibit such high Zr concentrations and are usually too mafic to crystallize zircon.

Limited-strain analysis carried out by Smith (2000) and in this study indicates that vertical shortening has occurred within the magma chamber during crystallization, which may also have contributed to crystal

alignment. Compaction is indicated by crenulated interfaces that lie perpendicular to the north–south direction of shortening (see Fig. 4c), and mafic enclaves that appear to have been compressed beneath dense mafic sheets above them (Fig. 2e). Crenulated margins will form if the mafic enclave is more viscous than the surrounding intermediate–felsic magma at the time of compression. Smith (2000) calculated that at least 50% shortening had occurred within the chamber, but this was based on calculations taken only from Evening Cove and is not representative of the entire sequence. Compaction is localized, with variable amounts of shortening throughout the chamber. This variation implies that shortening was not experienced at one single time throughout the chamber, but instead occurred episodically, most probably in response to loading of the chamber from mafic magma input and gravitational settling from above. Areas that have experienced a high degree of shortening probably had larger inputs of mafic magma above, resulting in magma loading, than areas that display a small degree of shortening. Areas that experienced high amounts of shortening are characterized by a high degree of mafic enclave abundance relative to the felsic host, with enclaves separated by very small amounts of felsic material, such that the two materials have moulded around each other. Mafic enclaves are also typically flattened and have high aspect ratios. The amount of shortening is probably also dependent on how soon after mafic enclave emplacement the overlying mafic sheet was injected. Mafic enclaves that preserve evidence for shortening would need to have been in a mushy state to accommodate the strain plastically.

The degree of crystallization of both the host and mafic magma plays an important role in allowing crystal accumulation and magmatic flow to occur, and in determining the amount of shortening preserved. Magma containing <20% crystals is able to accommodate magmatic flow and rotation of single crystals (Vigneresse *et al.*, 1996), and hence preserve magmatic flow textures and allow crystal settling to occur. Magmatic flow is still achievable in magmas with as much as 55% crystals; however, once above 55% crystals, foliations will develop only by solid-state processes (Vigneresse *et al.*, 1996). Once crystallinities have reached ~72–75% the magma is effectively solid, and will not accommodate shortening or magmatic flow as readily as a magma that contains fewer crystals. Melt fractions in excess of 50% were therefore likely within the intermediate–felsic host magmas of the Halfmoon Pluton, to allow for crystal accumulation and the flow of plagioclase crystals and mafic enclaves (Vernon *et al.*, 1988; Vigneresse *et al.*, 1996).

Fractional crystallization

The observed geochemical trends within the mafic and felsic rocks of the Halfmoon Pluton are consistent with fractional crystallization, which was likely to have been the dominant petrogenetic process during compositional differentiation. The magma composition of the intermediate-felsic host-rocks became progressively more silicic, changing from an intermediate leucodiorite (SiO_2 55%) towards the base of the chamber at AP and EC, to a tonalite–granodiorite (SiO_2 75%) towards the top of the chamber at RR and TN. Figure 9 shows the change in SiO_2, CaO, Al_2O_3 and Sr abundances with stratigraphic height in the chamber. These compositional changes are at least consistent with fractional crystallization, and were probably driven by the crystallization and accumulation of a plagioclase–hornblende–magnetite–zircon ± biotite mineral assemblage. Small variations in major and trace element abundances in the host leucodiorites at AP and EC can be attributed to the presence of trapped liquid within these cumulates, combined with the effect of minor fractional crystallization and limited mixing with the intruding mafic magma. Variable host-rock compositions within the Tottabetsu Igneous Complex have also been interpreted to have formed as a combination of these processes (Kamiyama *et al.*, 2007). Both field and petrographic evidence demonstrate that crystallization was interrupted episodically by large volumes of mafic magma replenishment in several discrete episodes throughout the history of the pluton. The effect of mafic magma replenishment on the composition of the host-rocks is reflected in fluctuating major element trends. Similar trends are observed in the Kameruka Pluton, where mafic magma replenishment is interpreted to be responsible for causing reverse fractionation trends (Collins *et al.*, 2006). The intermediate–felsic host and mafic rocks identified in the Halfmoon Pluton are themselves most probably the fractional crystallization products of a primitive basaltic parent. SiO_2 concentrations within the mafic rocks remain uniform, suggesting that all the mafic rocks represent repeated tapping of a mafic magma reservoir at depth that was recharging with magma of uniform composition.

Chemical exchange and mixing

As discussed in the isotopes section, there is very little evidence to suggest that complete chemical and isotopic equilibration occurred between the interacting mafic and intermediate–felsic rocks, as the intermediate–felsic host-rocks often display more primitive $^{87}Sr/^{86}Sr$ and ε_{Nd} than the mafic sheets and enclaves. The mafic enclaves are, however, enriched in the more mobile elements (Na_2O, K_2O, P_2O_5, Rb, Ba, Y) relative to the thicker mafic sheets and later cross-cutting mafic dikes that are inferred to represent the parent magma composition from which they originated. This probably reflects diffusion of these more mobile elements from the host magma into the mafic enclaves. Mafic enclaves within the Adamello Massif were shown by Blundy & Sparks (1992) to be enriched in trace and mobile elements relative to the enclosing host-rock, which they attributed to diffusion of these

elements from the melt phase of the enclosing host into the mafic enclave. No enrichment in these elements is observed within the mafic sheets and dikes, which indicates that these larger volume bodies were not affected by diffusion, probably because they chilled more rapidly and developed fine-grained margins that inhibited the diffusion of elements. Mafic enclaves also display a slight enrichment in MnO and Zn, which was attributed by Blundy & Sparks (1992) to represent equilibrium between the Fe–Ti oxides in the mafic enclaves and the host. Diffusion of elements between the mafic and felsic magmas is most likely to occur while both the enclave and host have high proportions of liquid, and therefore probably occurs immediately after the mafic enclaves have quenched.

MODEL OF MAGMA CHAMBER CONSTRUCTION AND EVOLUTION

The Halfmoon Pluton preserves multiple lines of evidence indicating that it was constructed incrementally from the base up, consisting of an aggrading crystal-rich intermediate cumulate mush at the base of the chamber and an overlying crystal-poor evolved felsic magma. Evidence indicating the Halfmoon Pluton was a single magma chamber constructed from the base up includes the following: (1) intrusive internal contacts are absent (excluding late highly evolved granite dikes and sheets); (2) orientations of mafic sheets and enclave swarms within the chamber are consistent with incremental growth from the base up; (3) U/Pb dates all overlap within error, indicating that the magmas were all active during a period not exceeding ~3 Myr; (4) pressure estimates based on hornblende compositions all overlap within error, indicating that the various rocks crystallized at depths between 4 and 10 km depth.

The paleo-floor within the chamber can be defined at any one time by each mafic sheet or enclave horizon that was injected at the boundary between the crystal-rich base and the crystal-poor magma above. The size of the active portion of the magma chamber at any one time during its crystallization history was likely to have been much smaller than the final overall size of the pluton. Plutons have been conceived by many workers (Glazner *et al.*, 2004; Miller & Wooden, 2004; Bachmann *et al.*, 2007) to contain portions that are melt-rich and melt-poor, and may consist of several adjacent melt pods that constitute a single magmatic system. Within the Halfmoon Pluton at least two separate melt 'pods' are recognized. The rocks at The Neck display contrasting mingling styles and orientations to the rest of the rocks within the Halfmoon Pluton. These are therefore interpreted to represent a younger adjacent melt 'pod' that was part of the same active system, as they have identical chemical and isotopic characteristics.

Limited isotopic variability across the entire petrological range within the Halfmoon Pluton suggests that all the rocks within the pluton are related petrogenetically. Whole-rock geochemistry, primitive isotopic signatures ($^{87}Sr/^{86}Sr_{(i)}$ range between 0·70379 and 0·70427 and ε_{Nd} range between +3·5 and +1·9) and a paucity of inherited zircons indicate that the Halfmoon Pluton rocks have undergone very little, if any, crustal contamination. Two mechanisms may explain the generation of intermediate–felsic magmas without the addition of continental crust: (1) fractional crystallization of mantle-derived basaltic magmas, or (2) partial melting of relatively young primitive lower crustal mafic–intermediate rocks of mantle derivation.

Tamura & Tatsumi (2002) suggested that rhyolite magmas within the Izu–Bonin Arc are produced by dehydration melting of calc-alkaline andesite in the upper to middle crust. It is possible that crustal melting of isotopically primitive plutonic rocks could have occurred to produce the Halfmoon Pluton rocks. Subduction along the paleo-Pacific margin of Gondwana was long-lived, and generated large volumes of plutonic bodies that are now exposed in the Median Batholith. The Halfmoon Pluton itself is incorporated into the composite Bungaree Intrusives, which were active from at least ~175 Ma to ~135 Ma. If the Halfmoon Pluton magmas were generated by partial melting of primitive Median Batholith plutonic rocks, this would require the presence of older material melted at mid-crustal depths, as partial melting of a deeper mafic protolith would result in an adakitic signature (Muir *et al.*, 1998), which is not observed within the rocks of the Halfmoon Pluton. Rocks with high Sr/Y ratios are interpreted to be the result of plagioclase accumulation and not from remelting a mafic protolith.

Scattered, curvilinear trends on Harker diagrams and petrographic textures indicate that fractional crystallization and crystal accumulation of a plagioclase–hornblende–zircon mineral assemblage probably played the most important role in generating the observed chemical diversity within the rocks of the Halfmoon Pluton. A system is envisaged in which hydrous amphibole-rich basaltic magmas pond at the crust–mantle interface and episodically rise, inject and mingle with an overlying intermediate–felsic magma chamber. This intermediate–felsic magma chamber is likely to represent the extracted evolved melt from the underplated mafic magma (i.e. Bachmann & Bergantz, 2004). The presence of cross-cutting mafic dikes with varying forms and compositions indicates that they were injected at different stages during pluton growth and crystallization, and is evidence for the continuous input of mafic magma into the magma chamber throughout its crystallization history.

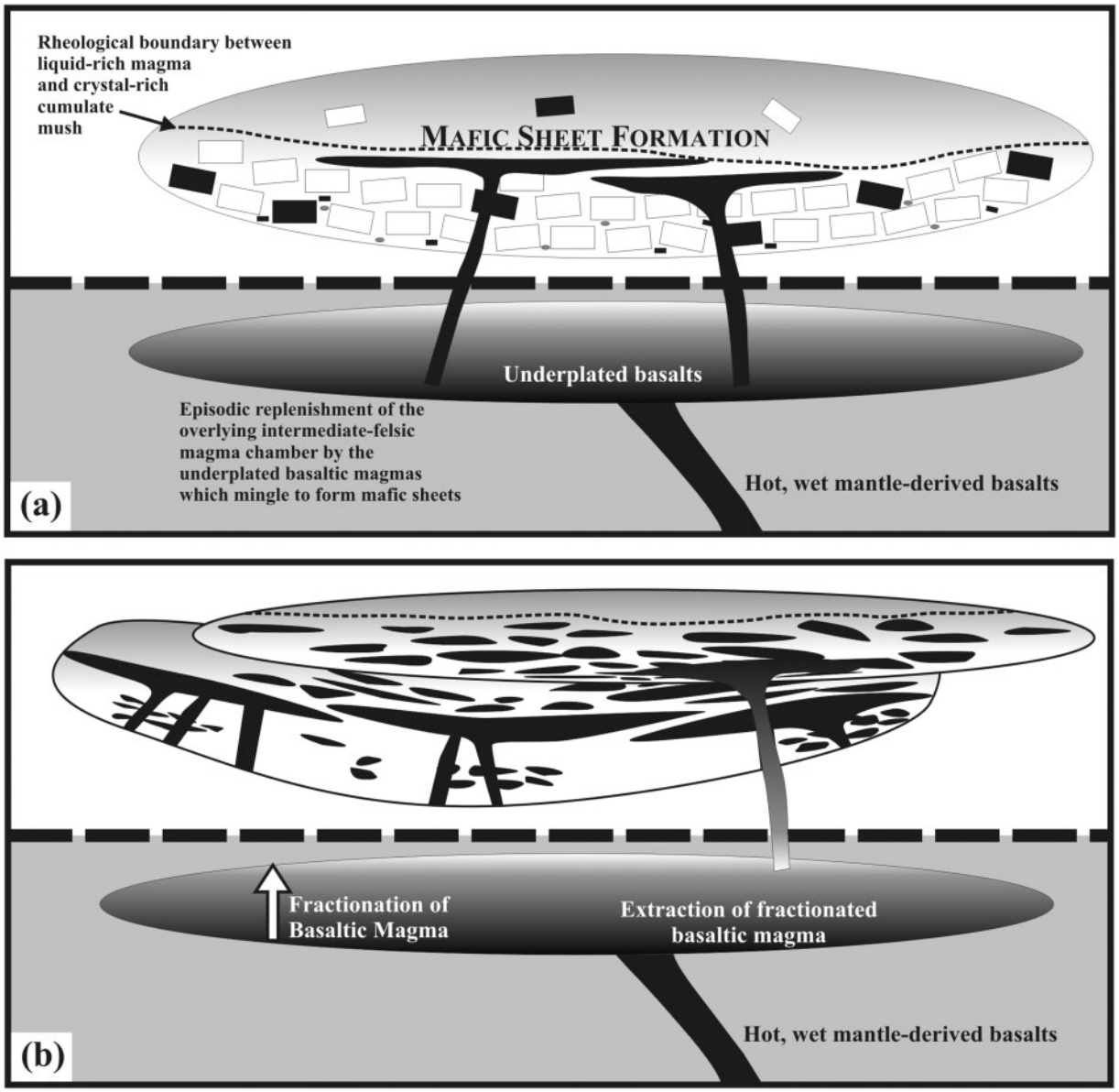

Fig. 11. Schematic diagrams illustrating the generation and evolution of the Halfmoon Pluton. (a) Accumulation and crystallization of a plagioclase (white crystals), hornblende (black crystals) and zircon (small grey crystals) mineral assemblage towards the inferred base of the chamber (Ackers Point and Evening Cove). Crystals are not to scale. Crystal settling and compaction creates a compositional gradient within the upper-crustal chamber. Hot, water-rich basaltic magma sourced from the underplated basaltic reservoir intermittently rises and injects into the crystal mush at the base of the chamber and spreads laterally at the rheological boundary with the overlying liquid-rich magma. These basaltic magmas quench and mingle to form mafic sheets and enclaves. (b) Extraction of interstitial melt from the chamber outlined in (a), and further injection of basaltic magma from the lower crustal reservoir forms an adjacent magmatic 'pod' at The Neck. Basaltic magma replenishment forms mafic enclave swarms.

A model for the construction and evolution of the Halfmoon Pluton is outlined below, and displayed in highly schematic diagrams in Fig. 11.

(1) Partial melting in the mantle wedge as a result of H_2O-rich fluids or melts released from the subducted slab generates the initial pulse of 'wet' primitive basaltic magma (i.e. Annen *et al.*, 2006). These mafic melts pond at the crust–mantle horizon. Fractional crystallization and extraction of interstitial liquid from the basaltic magmas forms the initial host magma chamber of the Halfmoon Pluton at mid- to upper-crustal levels. Early injections from dike-fed mafic magmas into the intermediate host magma

chamber when it was still relatively hot and crystal-poor would have undergone mixing and homogenization, and increased the overall size of the active chamber.

(2) Underplated amphibole-rich basaltic magmas rise episodically into the crust, inject into the base of the aggrading and fractionating host magma chamber, and mingle to form mafic sheets (Ackers Point and Evening Cove) (Fig. 11a). Increasing SiO_2 contents and decreasing MgO and CaO contents with 'stratigraphic' height in the chamber indicate that the mafic sheets, enclaves and dikes that injected into the Halfmoon Pluton have probably themselves been fractionated from the primitive basaltic melts ponded at the base of the crust.

(3) Fractionation of the underplated basaltic magmas has the effect of increasing the SiO_2 content of these basalts. Further replenishment of the intermediate–felsic magma chamber by these basaltic melts results in the formation of mafic enclave swarms (Ringaringa). Mafic enclaves are subsequently transported and aligned parallel to the mafic sheet orientations via magmatic currents operating within the crystal-poor felsic magma immediately above the cumulate mush.

(4) Differences in the strike and dip of the mafic enclaves or sheets at The Neck suggest that they represent an adjacent magma 'pod'. The inferred base of the pluton, represented by rocks at AP, EC and RR, is theorized to have cooled and mafic sheets or enclaves to have sunk and settled within the host magma. Compaction of the chamber in response to the intrusion of mafic magmas at higher levels may also have occurred. Extraction of interstitial melt and a possible return to a high influx of mafic magma form the adjacent magma 'pod' at The Neck.

(5) Episodic injection of basaltic magma into this felsic host magma chamber results in the formation of a thick succession of mafic enclaves (Fig. 11b). Intruding mafic magmas may have brought up pieces of partially crystallized hybrid mush from the base of the chamber, forming composite enclaves.

(6) The Halfmoon Pluton cooled sufficiently such that composite dikes intruded in brittle conditions. Composite dikes are concentrated at the top of the chamber (The Neck) where residual felsic melt would have still been present to be incorporated into the dikes.

(7) Following complete crystallization of the Halfmoon Pluton, late-stage granitic dikes and sheets with a more evolved whole-rock chemistry and isotopic signature were intruded, coupled with further mafic magma intrusion in the form of cross-cutting mafic dikes. Several mafic dikes intruded into the granite sheets, and disaggregated to form enclaves. Cross-cutting mafic dikes have identical chemistry and isotopic signature to the mafic sheets at Ackers Point and Evening Cove, indicating that under-plated basaltic magmas continued to intrude into the Halfmoon Pluton even after it was largely solidified.

CONCLUSIONS

Field and petrographic relationships, and geochemical and geochronological data lead to the following conclusions regarding the origin and evolution of the Halfmoon Pluton.

(1) The Halfmoon Pluton represents an intermediate–felsic crustal magma chamber that was episodically replenished by mantle-derived mafic magmas that mingled and mixed locally and at depth.

(2) Widespread south-dipping sheets and rare tilted felsic pipes are interpreted as paleohorizontal pluton features that were subsequently tilted to the south. Way-up structures and textures within the Halfmoon Pluton are consistent with a younging direction to the south, allowing a magma chamber 'stratigraphy' to be constructed.

(3) Mingling styles vary according to position within the inferred chamber as a result of such factors as temperature, viscosity, relative volumes, compositional contrasts, volatile content, and rate of replenishment. Fine-grained chilled contacts of mafic sheets and enclaves indicate that mingling was favoured over mixing, largely because of substantial temperature and viscosity contrasts between the two interacting magmas.

(4) The intermediate–felsic host-rocks evolved through crystal accumulation and fractional crystallization of a plagioclase–hornblende–zircon mineral assemblage that was frequently interrupted by injections of mafic magma.

(5) The mingled mafic and felsic rocks are probably genetically related, as both have very similar modal mineralogy, mineral composition, chemical composition and isotopic compositions. Their geochemical similarity and proximity in space and time indicate that the system can be classified as a single composite pluton, with different portions active at different times.

(6) The calc-alkaline, I-type Halfmoon Pluton was generated within a primitive arc setting, most probably an island-arc setting, as it preserves no evidence for any contamination by old continental crust.

Processes identified within the Halfmoon Pluton are thus directly analogous to active arc settings, and therefore provide perspectives on the origin and evolution of arc magmas, including: (1) physico-chemical processes of crystal accumulation, crystal–liquid separation, compaction, magma mingling and mixing and fractional crystallization; (2) mid- to upper-crustal magma chambers

commonly characterized by mafic magma replenishment; (3) evolution of magmas within arc settings to intermediate and silicic compositions by fractionation and crystal accumulation, and subsequent extraction of evolved melts, without any significant crustal assimilation.

ACKNOWLEDGEMENTS

Research was carried out while R.T. held a New Zealand Top Achiever Doctoral Scholarship. R.T. thanks Bob Wiebe for help in the field and for providing insightful comments throughout the course of research. Bill Collins, Calvin Miller and Richard Price are thanked for thorough and insightful reviews that greatly improved the content of this paper. Editor John Gamble is thanked for comments which improved the clarity of this paper.

FUNDING

This research was supported by a grant to J.C. and S.W. from the Marsden Fund, administered by the Royal Society of New Zealand (UOC0508), and the Mason Trust Fund, Department of Geological Sciences, University of Canterbury.

REFERENCES

Allibone, A. H. & Tulloch, A. J. (2004). Geology of the plutonic basement rocks of Stewart Island, New Zealand. *New Zealand Journal of Geology and Geophysics* **47**, 233–256.

Allibone, A. H., Jongens, R., Scott, J. M., Tulloch, A. J., Turnbull, I. M., Cooper, A. F., Powell, N. G., Ladley, E. B., King, R. P. & Rattenbury, M. S. (2009). Plutonic rocks of the Median Batholith in eastern and central Fiordland, New Zealand: field relations, geochemistry, correlation, and nomenclature. *New Zealand Journal of Geology and Geophysics* **52**, 101–148.

Anderson, J. L. & Smith, D. R. (1995). The effects of temperature and $\times O_2$ on the Al-in-hornblende barometer. *American Mineralogist* **80**, 549–559.

Annen, C., Blundy, J. D. & Sparks, R. S. J. (2006). The genesis of intermediate and silicic magmas in deep crustal hot zones. *Journal of Petrology* **47**, 505–539.

Arculus, R. J. (1994). Aspects of magma genesis in arcs. *Lithos* **33**, 189–208.

Bachl, C. A., Miller, C. F., Miller, J. S. & Faulds, J. E. (2001). Construction of a pluton: Evidence from an exposed cross section of the Searchlight pluton, Eldorado Mountains, Nevada. *Geological Society of America Bulletin* **113**, 1213–1228.

Bachmann, O. & Bergantz, G. W. (2004). On the origin of crystal-poor rhyolites: extracted from batholithic crystal mushes. *Journal of Petrology* **45**, 1565–1582.

Bachmann, O., Miller, C. F. & de Silva, S. L. (2007). The volcanic–plutonic connection as a stage for understanding crustal magmatism. *Journal of Volcanology and Geothermal Research* **167**, 1–23.

Baker, D. R. (1996). Granitic melt viscosities: Empirical and configurational entropy models for their calculation. *American Mineralogist* **81**, 126–134.

Barbarin, B. & Didier, J. (1992). Genesis and evolution of mafic microgranular enclaves through various types of interaction between coexisting felsic and mafic magmas. *Transactions of the Royal Society of Edinburgh: Earth Sciences* **83**, 145–153.

Black, L. P., Kamo, S. L., Allen, C. M., Aleinikoff, J. N., Davis, D. W., Korsch, R. J. & Foudoulis, C. (2003). TEMORA 1: a new zircon standard for Phanerozoic U–Pb geochronology. *Chemical Geology* **200**, 155–170.

Blundy, J. D. & Holland, T. J. B. (1990). Calcic amphibole equilibria and a new amphibole–plagioclase geothermometer. *Contributions to Mineralogy and Petrology* **104**, 208–224.

Blundy, J. D. & Sparks, R. S. J. (1992). Petrogenesis of mafic inclusions in granitoids of the Adamello Massif, Italy. *Journal of Petrology* **33**, 1039–1104.

Campbell, I. H. & Turner, J. S. (1985). Turbulent mixing between fluids with different viscosities. *Nature* **313**, 39–42.

Coleman, D. S., Glazner, A. F., Miller, J. S., Bradford, K. J., Frost, T. P., Joye, J. L. & Bachl, C. A. (1995). Exposure of a Late Cretaceous layered mafic–felsic magma system in the central Sierra Nevada Batholith, California. *Contributions to Mineralogy and Petrology* **120**, 129–136.

Coleman, D. S., Gray, W. & Glazner, A. F. (2004). Rethinking the emplacement and evolution of zoned plutons: Geochronological evidence for incremental assembly of the Tuolumne Intrusive Suite, California. *Geology* **32**, 433–436.

Collins, W. J., Wiebe, R. A., Healy, B. & Richards, S. W. (2006). Replenishment, crystal accumulation and floor aggradation in the megacrystic Kameruka Suite, Australia. *Journal of Petrology* **47**, 2073–2104.

Cook, N. D. J. (1988). Diorites and associated rocks in the Anglem Complex at the Neck, northeastern Stewart Island, New Zealand: an example of magma mingling. *Lithos* **21**, 247–262.

Corfu, F., Hanchar, J. M., Hoskin, P. W. O. & Kinny, P. D. (2003). Atlas of zircon textures. In: Hanchar, J. M. & Hoskin, P. W. O. (eds) *Zircon. Mineralogical Society of America and Geochemical Society, Reviews in Mineralogy and Geochemistry* **53**, 469–500.

Davies, G. R., Halliday, A. N., Mahood, G. A. & Hall, C. M. (1994). Isotopic constraints on the production rates, crystallization histories and residence times of pre-caldera silicic magmas, Long Valley, California. *Earth and Planetary Science Letters* **125**, 17–37.

Deer, W. A., Howie, R. A. & Zussman, J. (1997). *Rock Forming Minerals, Volume 2B, Double Chain Silicates*, 2nd edn. Geological Society of London.

Frost, T. P. & Mahood, G. A. (1987). Field, chemical, and physical constraints on mafic–felsic magma interaction in the Lamarck Granodiorite, Sierra Nevada, California. *Geological Society of America Bulletin* **99**, 272–291.

Glazner, A. F., Bartley, J. M., Coleman, D. S., Gray, W. & Taylor, R. Z. (2004). Are plutons assembled over millions of years by amalgamation from small magma chambers? *GSA Today* **14**, 4–11.

Hammarstrom, J. M. & Zen, E-A. (1986). Aluminium in hornblende: An empirical igneous geobarometer. *American Mineralogist* **71**, 1297–1313.

Harper, B. E., Miller, F., Miller, G., Koteas, C., Cates, N. L., Wiebe, R. A., Lazzareschi, D. S. & Cribb, J. W. (2004). Granites, dynamic magma chamber processes and pluton construction: the Aztec Wash pluton, Eldorado Mountains, Nevada, USA. *Transactions of the Royal Society of Edinburgh: Earth Sciences* **95**, 277–295.

Hawkins, D. P. & Wiebe, R. A. (2004). Discrete stoping events in granite plutons: a signature of eruptions from silicic magma chambers? *Geology* **32**, 1021–1024.

Holland, T. & Blundy, J. (1994). Non-ideal interactions in calcic amphiboles and their bearing on amphibole–plagioclase thermometry. *Contributions to Mineralogy and Petrology* **116**, 433–447.

Hollister, L. S., Grissom, G. C., Peters, E. K., Stowell, H. H. & Sisson, V. B. (1987). Confirmation of the empirical correlation of Al in hornblende with pressure of solidification of calc-alkaline plutons. *American Mineralogist* **72**, 231–239.

Hoskin, P. W. O. & Schaltegger, U. (2003). The composition of zircon and igneous and metamorphic petrogenesis. In: Hanchar, J. M. & Hoskin, P. W. O. (eds) *Zircon. Mineralogical Society of America and Geochemical Society, Reviews in Mineralogy and Geochemistry* **53**, 27–62.

Jellinek, A. M. & DePaolo, D. J. (2003). A model for the origin of large silicic magma chambers: precursors of caldera-forming eruptions. *Bulletin of Volcanology* **65**, 363–381.

Johnson, M. C. & Rutherford, M. J. (1989). Experimentally determined conditions in the Fish Canyon Tuff, Colorado, magma chamber. *Journal of Petrology* **30**, 711–737.

Kamiyama, H., Nakajima, T. & Kamioka, H. (2007). Magmatic stratigraphy of the tilted Tottabetsu Plutonic Complex, Hokkaido, North Japan: magma chamber dynamics and pluton construction. *Journal of Geology* **115**, , 295–314.

Kimbrough, D. L., Tulloch, A. J., Coombs, D. S., Landis, C. A., Johnston, M. R. & Mattinson, J. M. (1994). Uranium–lead zircon ages from the Median Tectonic Zone, New Zealand. *New Zealand Journal of Geology and Geophysics* **37**, 393–419.

Leake, B. E. & Said, Y. A. (1994). Hornblende barometry of the Galway Batholith, Ireland: an empirical test. *Mineralogy and Petrology* **51**, 1438–1168.

Leake, B. E., Woolley, A. R., Arps, C. E. S. *et al.* (1997). Nomenclature of amphiboles: Report of the subcommittee on amphiboles of the international mineralogical association, commission on new minerals and mineral names. *Canadian Mineralogist* **35**, 219–246.

Lipman, P. W. (2007). Incremental assembly and prolonged consolidation of Cordilleran magma chambers: Evidence from the Southern Rocky Mountain volcanic field. *Geosphere* **3**, 42–70.

McCulloch, M. T. (1993). The role of subducted slabs in an evolving Earth. *Earth and Planetary Science Letters* **115**, 89–100.

Miller, C. F. & Miller, J. S. (2002). Contrasting stratified plutons exposed in tilt blocks, Eldorado Mountains, Colorado River Rift, NV, USA. *Lithos* **61**, 209–224.

Miller, J. S. & Wooden, J. L. (2004). Residence, resorption and recycling of zircons in Devils Kitchen Rhyolite, Coso Volcanic Field, California. *Journal of Petrology* **45**, 2155–2170.

Mortimer, N., Tulloch, A. J., Spark, R. N., Walker, N. W., Ladley, E., Allibone, A. & Kimbrough, D. L. (1999). Overview of the Median Batholith, New Zealand: a new interpretation of the geology of the Median Tectonic Zone and adjacent rocks. *Journal of African Earth Sciences* **29**, 257–268.

Muir, R. J., Ireland, T. R., Weaver, S. D., Bradshaw, J. D., Waight, T. E., Jongens, R. & Eby, G. N. (1997). SHRIMP U–Pb geochronology of Cretaceous magmatism in northwest Nelson–Westland, South Island, New Zealand. *New Zealand Journal of Geology and Geophysics* **40**, 453–463.

Muir, R. J., Ireland, T. R., Weaver, S. D., Bradshaw, J. D., Evans, J. A., Eby, G. N. & Shelley, D. (1998). Geochronology and geochemistry of a Mesozoic magmatic arc system, Fiordland, New Zealand. *Journal of the Geological Society, London* **155**, 1037–1053.

Perugini, D., Poli, G. & Rocchi, S. (2005). Development of viscous fingering between mafic and felsic magmas: evidence from the Terra Nova Intrusive Complex (Antarctica). *Mineralogy and Petrology* **83**, 151–166.

Poli, G., Tommasini, S. & Halliday, A. N. (1996). Trace element and isotopic exchange during acid–basic magma interaction processes. *Transactions of the Royal Society of Edinburgh: Earth Sciences* **87**, 225–232.

Ridolfi, F., Renzulli, A. & Puerini, M. (2010). Stability and chemical equilibrium of amphibole in calc-alkaline magmas: an overview, new thermobarometric formulations and application to subduction-related volcanoes. *Contributions to Mineralogy and Petrology*, doi:10.1007/s00410-009-0465-7.

Scaillet, B., Holtz, F. & Pichavant, M. (1998). Phase equilibrium constraints on the viscosity of silicic magmas. 1. Volcanic–plutonic comparison. *Journal of Geophysical Research* **103**, 27257–27266.

Schmidt, M. W. (1992). Amphibole composition in tonalite as a function of pressure: an experimental calibration of the Al-in-hornblende barometer. *Contributions to Mineralogy and Petrology* **110**, 304–310.

Shukuno, H., Tamura, Y., Tani, K., Chang, Q., Suzuki, T. & Fiske, R. S. (2006). Origin of silicic magmas and the compositional gap at Sumisu submarine caldera, Izu–Bonin arc, Japan. *Journal of Volcanology and Geothermal Research* **156**, 187–216.

Smith, I. E. M., Worthington, T. J., Stewart, R. B., Price, R. C. & Gamble, J. A. (2003). Felsic volcanism in the Kermadec arc, southwest Pacific: crustal recycling in an oceanic setting. In: Larter, R. D. & Leat, P. T. (eds) *Intra-oceanic Subduction Systems: Tectonic and Magmatic Processes. Geological Society, London, Special Publication* **219**, 99–118.

Smith, I. E. M., Worthington, T. J., Price, R. C., Stewart, R. B. & Maas, R. (2006). Petrogenesis of dacite in an oceanic subduction environment: Raoul Island, Kermadec arc. *Journal of Volcanology and Geothermal Research* **156**, 252–265.

Smith, J. V. (2000). Structures of interfaces of mingled magmas, Stewart Island, New Zealand. *Journal of Structural Geology* **22**, 123–133.

Snyder, D. & Tait, S. (1995). Replenishment of magma chambers: comparison of fluid-mechanic experiments with field relations. *Contributions to Mineralogy and Petrology* **122**, 230–240.

Snyder, D., Crambes, C., Tait, S. & Wiebe, R. A. (1996). Magma mingling in dikes and sills. *Journal of Geology* **105**, 75–86.

Sparks, R. J. & Marshall, L. (1986). Thermal and mechanical constraints on mixing between mafic and silicic magmas. *Journal of Volcanology and Geothermal Research* **29**, 99–124.

Streckeisen, A. L. (1973). Classification and nomenclature recommended by the IUGS subcommission on the systematics of igneous rocks. *Geotimes* **10**, 26–31.

Tamura, Y. & Tatsumi, Y. (2002). Remelting of an andesitic crust as a possible origin for rhyolite magma in oceanic arcs: an example from Izu–Bonin Arc. *Journal of Petrology* **43**, 1029–1047.

Tamura, Y., Gill, J. B., Tollstrup, D., Kawabata, H., Shunkuno, H., Chang, Q., Miyazaki, T., Takahashi, T., Hirahara, Y., Kodaira, S., Ishizuka, O., Suzuki, T., Kido, Y., Fiske, R. S. & Tatsumi, Y. (2009). Silicic magmas in the Izu–Bonin oceanic arc and implications for crustal evolution. *Journal of Petrology* **50**, 685–723.

Thomas, W. M. & Ernst, W. G. (1990). The aluminium content of hornblende in calc-alkaline granitic rocks: a mineralogic barometer calibrated experimentally to 12 kbars. In: Spencer, R. J. & Chou, I.-M. (eds) *Fluid–Mineral Interactions: a Tribute to H. P. Eugster. Geochemical Society Special Publication* **2**, 59–63.

Tulloch, A. J. & Kimbrough, D. L. (2003). Paired plutonic belts in convergent margins and the development of high Sr/Y magmatism: Peninsular Ranges batholith of Baja-California and Median batholith of New Zealand. In: Johnson, S. E., Paterson, S. R., Fletcher, J. M., Girty, G. H., Kimbrough, D. L. & Martin-Barajas, A. (eds) *Tectonic Evolution of Morthwestern Mexico and the Southwestern USA. Geological Society of America, Special Papers* **374**, 275–295.

Ulfbeck, D., Baker, J., Waight, T. & Krogstad, E. (2003). Rapid sample digestion and chemical separation of Hf for isotopic analysis by MC-ICPMS. *Talanta* **59**, 365–373.

Vernon, R. H., Etheridge, M. A. & Wall, V. J. (1988). Shape and microstructure of microgranitoid enclaves: indicators of magma mingling and flow. *Lithos* **22**, 1–11.

Vigneresse, J. L., Barbey, P. & Cuney, M. (1996). Rheological transitions during partial melting and crystallization with application to felsic magma segregation and transfer. *Journal of Petrology* **37**, 1579–1600.

Waight, T. E., Wiebe, R. A., Krogstad, E. J. & Walker, R. J. (2001). Isotopic response to basaltic injections into silicic magma chambers; a whole-rock and microsampling study of macrorhythmic units in the Pleasant Bay layered gabbro–diorite complex, Maine, USA. *Contributions to Mineralogy and Petrology* **142**, 323–335.

Waight, T. E., Baker, J. A. & Peate, D. W. (2002). Sr isotope ratio measurements by double-focusing MC-ICPMS: techniques, observations and pitfalls. *International Journal of Mass Spectrometry* **221**, 229–244.

Walker, B. A., Miller, C. F., Claiborne, L. L., Wooden, J. L. & Miller, J. S. (2007). Geology and geochronology of the Spirit Mountain batholith, southern Nevada: implications for timescales and physical processes of batholith construction. *Journal of Volcanology and Geothermal Research* **167**, 239–262.

Watters, W. A. (1978). Diorite and associated intrusive and metamorphic rocks between Port William and Paterson Inlet, Stewart Island, and on Ruapuke Island. *New Zealand Journal of Geology and Geophysics* **21**, 423–442.

Weaver, S. D., Gibson, I. L., Houghton, B. F. & Wilson, C. J. N. (1990). Mobility of rare earth and other elements during crystallization of peralkaline silicic lavas. *Journal of Volcanology and Geothermal Research* **43**, 57–70.

Wiebe, R. A. (1973). Relations between coexisting basaltic and granitic magmas in a composite dike. *American Journal of Science* **273**, 130–151.

Wiebe, R. A. (1993*a*). The Pleasant Bay layered gabbro–diorite, Coastal Maine: Ponding and crystallization of basaltic injections into a silicic magma chamber. *Journal of Petrology* **34**, 461–489.

Wiebe, R. A. (1993*b*). Basaltic injections into floored silicic magma chambers. *EOS Transactions, American Geophysical Union* **74**, 1–4.

Wiebe, R. A. (1994). Silicic magma chambers as traps for basaltic magmas: the Cadillac Mountain intrusive complex, Mount Desert Island, Maine. *Journal of Geology* **102**, 423–437.

Wiebe, R. A. (1996). Mafic–silicic layered intrusions: the role of basaltic injections on magmatic processes and the evolution of silicic magma chambers. *Transactions of the Royal Society of Edinburgh: Earth Sciences* **87**, 233–242.

Wiebe, R. A. & Collins, W. J. (1998). Depositional features and stratigraphic sections in granitic plutons: implications for the emplacement and crystallization of granitic magma. *Journal of Structural Geology* **20**, 1273–1289.

Wiebe, R. A. & Ulrich, R. (1997). Origin of composite dikes in the Gouldsboro granite, coastal Maine. *Lithos* **40**, 157–178.

Wiebe, R. A., Frey, H. & Hawkins, D. P. (2001). Basaltic pillow mounds in the Vinalhaven intrusion, Maine. *Journal of Volcanology and Geothermal Research* **107**, 171–184.

Wiebe, R. A., Blair, K. D., Hawkins, D. P. & Sabine, C. P. (2002). Mafic injections, *in situ* hybridization, and crystal accumulation in the Pyramid Peak granite, California. *Geological Society of America Bulletin* **114**, 909–920.

Wright, I. C., Worthington, T. J. & Gamble, J. A. (2006). New multibeam mapping and geochemistry of the 30°–35°S sector, and overview, of southern Kermadec arc volcanism. *Journal of Volcanology and Geothermal Research* **149**, 263–296.